ACCELERATED FATIGUE RELIABILITY ANALYSIS OF STIFFENED SECTIONS USING DEEP LEARNING

By

HAIDER ALI

Bachelor of Science in Civil Engineering

National University of Sciences and Technology

Islamabad, Pakistan

2014

Submitted to the Faculty of the
Graduate College of the
Oklahoma State University
in partial fulfillment of
the requirements for
the Degree of
MASTER OF SCIENCE
December, 2018

ACCELERATED FATIGUE RELIABILITY

ANALYSIS OF STIFFENED SECTIONS

USING DEEP LEARNING

Thesis Approved:

Dr. Mohamed Soliman

Thesis Adviser

Dr. Bruce W. Russell

Dr. Julie A. Hartell

ACKNOWLEDGEMENTS

I would like to thank my academic advisor Dr. Mohamed Soliman, whose continuous guidance and support has led me to successfully complete my research and thesis. I am grateful for all the opportunities that Dr. Soliman has provided for me during my two years at Oklahoma State University. I want to thank my committee members Dr. Russell and Dr. Hartell, for taking the time to review my work and for providing valuable feedback. I would also like to thank the colleagues and friends, Christopher Waite, Ligang Sheng for their support and encouragement and Omid Khandel for helping me with my research work and providing feedback. I thank my loving parents whose unconditional love, support and constant reassurance has made me the person that I am today. I am unable to express in words my respect and love for them. I would like to also thank my uncle, Shahjahan Ali and his family for always being there and providing moral support. Last but not the least, I want to thank my beautiful and loving wife Anum, who always believed in me and encouraged and inspired me to aim higher. She has been extremely helpful throughout the course of my degree.

Name: HAIDER ALI

Date of Degree: DECEMBER, 2018

Title of Study: ACCELERATED FATIGUE RELIABILITY OF STIFFENED SECTIONS USING DEEP LEARNING

Major Field: CIVIL ENGINEERING

Abstract: Fatigue is one of the main failure mechanisms in structures subjected to fluctuating loads such as bridges and ships. If inadequately designed for such loads, fatigue can be detrimental to the safety of the structure. When fatigue cracks reach a certain size, sudden fracture failure or yielding of the reduced section can occur. Accordingly, quantifying the critical crack size is essential for determining the reliability of fatigue critical structures under growing cracks. Failure Assessment Diagrams (FADs) can be used to determine the critical crack size or whether the state of the crack is acceptable or not at a particular instant in time. Due to the presence of uncertainties in loads, material properties and crack growth behavior, probabilistic analysis is essential to understand the fatigue performance of the structure over its service life. A time dependent reliability profile for the structure can be established to help schedule maintenance and repair activities. However, probabilistic analysis of crack growth under complex geometrical and loading conditions can be very expensive computationally. Deep learning is a useful tool that is used in this study to curtail this lengthy process by establishing multi-variate non-linear approximations for complex fatigue crack growth profiles. This study proposes a framework for establishing the fatigue reliability profiles of stiffened panels under uncertainty. Monte Carlo simulation is used to draw samples from relevant probabilistic parameters and establish the time dependent reliability profile of the structure under propagating cracks. Deep learning is adopted to improve the computational efficiency of the probabilistic analysis in establishing the probabilistic crack growth profiles. The proposed framework is illustrated on a bridge with stiffened tub girders subjected to fatigue loading.

TABLE OF CONTENTS

Chapter Page

LIST OF TABLES

LIST OF FIGURES

Figure Page

Figure Page

CHAPTER I

INTRODUCTION AND LITERATURE REVIEW

Overview

Fatigue is one of the major factors governing the integrity of civil structures that are subjected to repetitive load cycles. Due to the presence of inherent discontinuities and flaws in the material, development of stress concentrations is imminent. These flaws can develop during manufacturing and fabrication or due to residual stresses induced during welding (Osgood, 1954). Although the loads experienced by structural members can be less than their yield strength, the stress concentrations at discontinuities and flaws may result in development of cracks. The repetitive stress cycles create plastic deformations at the crack tip causing crack growth to occur (Lu and Liu, 2010). If these growing cracks are not detected and repaired in a timely manner, sudden structure failure can occur (Han and Ramulu, 2005). The ASCE Committee on Fatigue Reliability determined that approximately 80% – 90% of the failures of steel structures are due to fracture and fatigue (ASCE Committee on Fatigue and Fracture Relibaility, 1982). Furthermore, the increase in the Average Daily Truck Traffic (ADTT) and truck loads over time (Nowak, 1993) results in an increase in the number and amplitude of stress cycles which can accelerate the crack growth. It is important to quantify the critical crack size at which structural failure can occur. The presence of uncertainties in traffic loads along with material properties and crack growth parameters necessitates the use of probabilistic approaches to better understand the structural

behavior under fatigue deterioration. Moreover, reliability and risk-based management techniques can be used to determine the safe service life of a structure and schedule timely maintenance and repair activities. In prior studies dealing with probabilistic fatigue analysis (Kwon et. al., 2012, Zhao et. al., 1994a, Cheung and Li, 2003), this crack size was assumed based on engineering judgement or taken as the maximum dimension available for the crack to grow into. In this study, Failure Assessment Diagram (FAD) is used to determine the critical crack size based on the loading conditions, geometry and material properties. Depending on the complexity of the geometry or loading conditions, traditional probabilistic analysis (such as Monte Carlo simulation) can be very expensive computationally. Deep learning is a promising supplementary tool that can aid in reducing the computational time associated with probabilistic analyses for complex geometries. In this study, deep learning is used to curb the computational expense and develop the probabilistic crack growth profiles. A performance function is defined to quantify the probability of failure under propagating fatigue cracks using Monte Carlo simulation. Finally, this probability of failure can be used to quantify the time variant reliability index.

Objectives

The main objective of this thesis is to develop a probabilistic framework for quantifying the reliability of stiffened panels under propagating cracks. This thesis employs an existing crack growth model to predict the fatigue crack growth in a panel with multiple welded longitudinal stiffeners and by assuming uncertainty in loads, material properties and crack growth parameters. In more detail, this study aims to:

- Determine the crack growth in a stiffened panel considering the effects of stiffener restraint, severed stiffeners and residual stresses on crack growth rate.
- Develop a probabilistic crack growth profile of a stiffened panel under fatigue loading using Monte Carlo simulation, considering uncertainties in material properties, loads and

crack growth model parameters. This will also serve as a training data set for the deep learning model.

- Train a deep learning algorithm based on the probabilistic crack growth data available from Monte Carlo simulation to accelerate the probabilistic simulation process.
- Utilize failure assessment diagrams to determine the probability distribution of the critical crack size at which the structure becomes unsafe for further use.
- Determine the probability of the crack size exceeding the critical crack size over time by using Monte Carlo simulation and subsequently determine the time variant reliability index.

Linear Elastic Fracture Mechanics (LEFM): A Brief Review

For studying the fatigue reliability of a critical detail, the S-N or crack growth approaches can be used. The S-N (stress-life) curve approach outlined in the AASHTO LRFD Bridge Design Specifications (AASHTO, 2017) can be used to estimate the fatigue life of different groups of structural details. However, these generalized curves cannot help in determining the state of the crack at a certain time. Linear Elastic Fracture Mechanics (LEFM) can be used to solve this problem and determine the crack size at a point in time. Three types of fracture failures can occur as shown in Figure 1. Mode I is referred to as opening, where the load is applied perpendicular to the crack surface. Mode II is called sliding and is caused by in-plane shear loading and Mode III is called tearing caused by out-of-plane shear loading. Mode I fracture mode will be covered in this study. LEFM uses the stress concentration ahead of the crack tipto study the crack behavior. This concentration described by the stress intensity factor expressed as (Xiao et. al., 2006)

$$K = F\sigma\sqrt{\pi a} \qquad \text{Eq. (1)}$$

where σ is the applied stress, a is the crack size and F is the geometry correction factor defined as

$$F = F_s F_t F_g F_e \qquad \text{Eq. (2)}$$

where F_s accounts for effects of free surface, F_t accounts for finite thickness or width, F_g accounts for non-uniform opening stress and F_e accounts for elliptical crack fronts (Albrecht and Yamada, 1977).

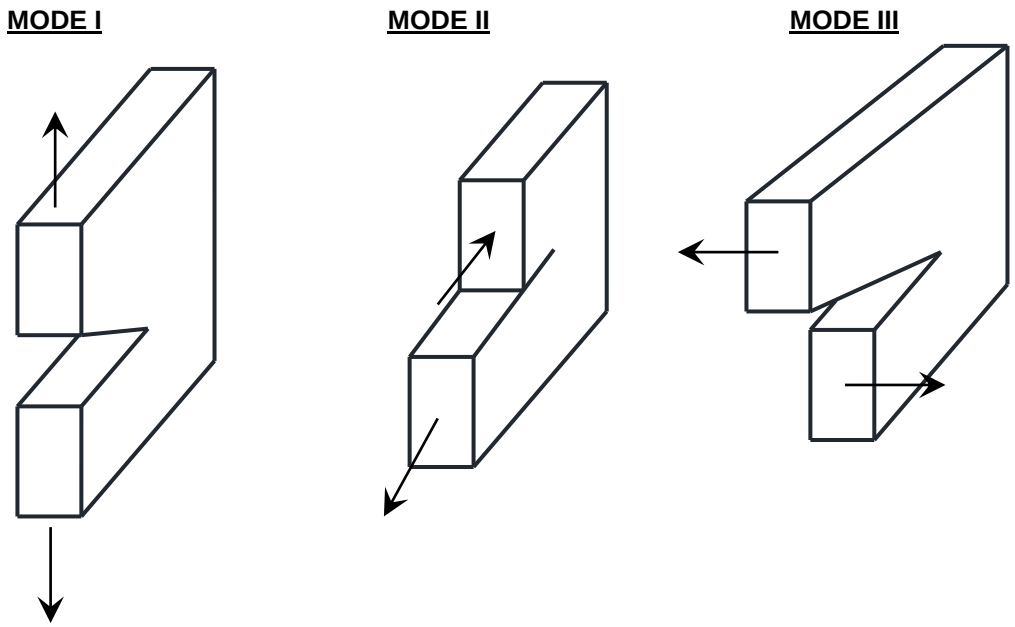

Fig. 1 - Modes of fracture failure

Fatigue crack growth occurs with fluctuating stress cycles. Paris and Erdogan (1963) established a relationship between the range of stress intensity factor, ΔK, and the rate of crack growth, da/dN, in logarithmic scale as shown in Figure 2. Based on experimental results it was observed that the crack growth rate can be divided into three regions. Slow crack growth takes place in region I when the range of stress intensity factor ΔK is smaller than a threshold value ΔK_{eff}. Performing a best fit of the plotted results, the crack growth rate was observed to vary linearly with the applied stress intensity factor range until the fracture toughness of the material was reached. In region III, the crack growth becomes unstable and results in sudden failure of the

specimen. The crack growth rate in region II is represented by the Paris law as (Paris and Erdogan, 1963)

$$\frac{da}{dN} = C \cdot \Delta K^m \qquad \text{Eq. (3)}$$

where C and m are material constants.

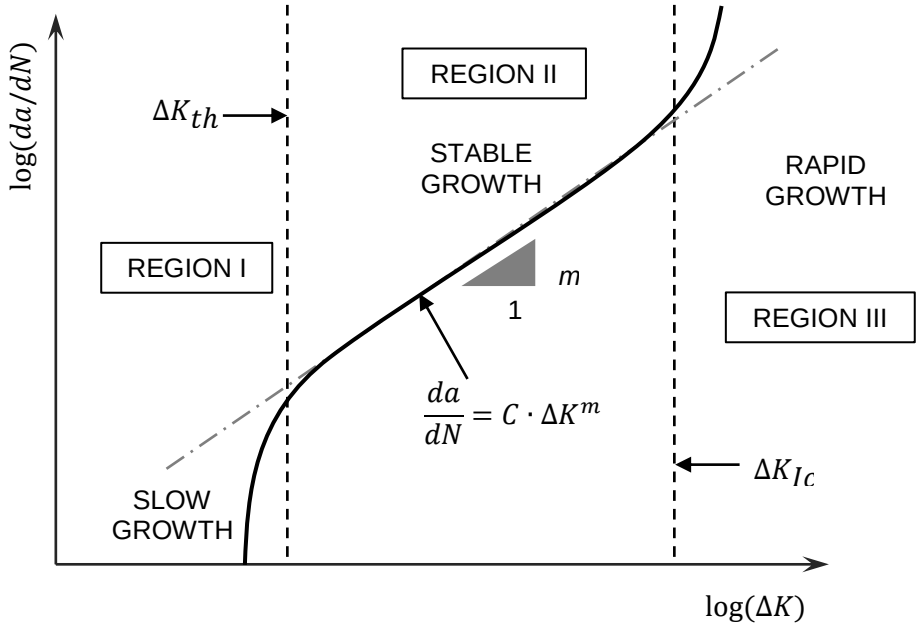

Fig. 2 - Paris law

Paris law provided a basic kernel for subsequent research in fatigue crack growth. Various formulations of ΔK exist in literature to determine the effect of applied loads on the crack growth and modify the crack growth model to account for variable amplitude loading. Under tensile loading, a plastic region develops ahead of the crack tip. When the tensile stress is removed, the plastic region remains deformed, and the surrounding material applies compressive forces on the plastic zone when unloaded elastically (Dexter and Pilarski, 2000). Elber (1971) determined that the compressive forces ahead of the plastically deformed zone can delay the crack opening up until a certain amount of tensile stress is reached. This phenomenon is called crack closure. Since

the crack will only grow if it is fully open, Elber proposed that an effective stress intensity factor ΔK_{eff} to be used instead of ΔK, which can be defined as

$$\Delta K_{eff} = K_{max} - K_{op} \qquad \text{Eq. (4)}$$

where K_{op} is stress intensity factor when the crack is fully open in the stress cycle. Figure 3 shows the different stress intensity factors that occur in a stress cycle.

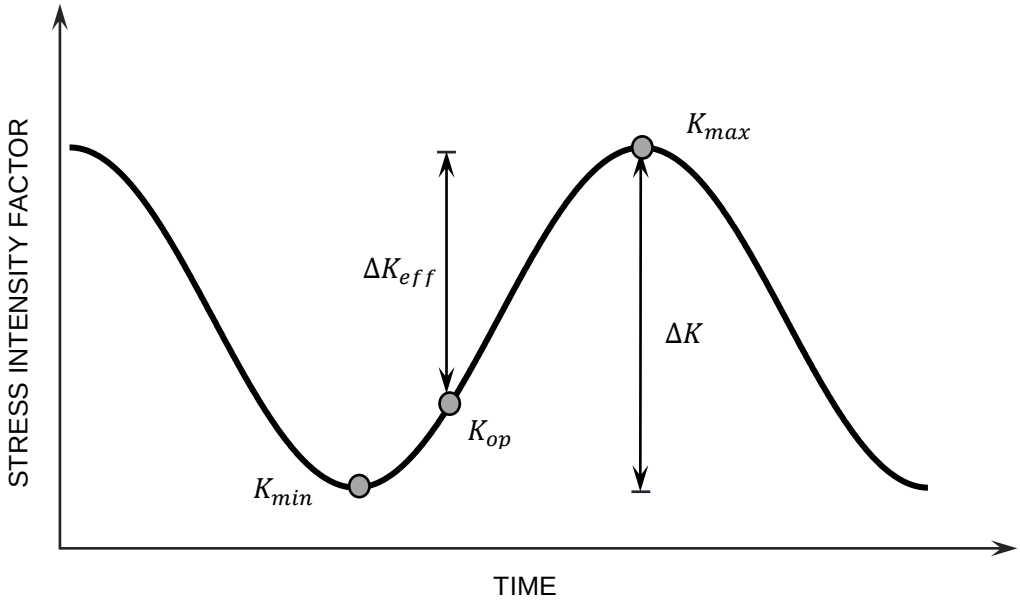

Fig. 3 - Stress cycle showing the different stress intensity factors

Fatigue Crack Growth Under Complex Loading

Various research studies have used LEFM to understand the behavior of fatigue cracks in different metals with various geometric configurations. McMillian and Pelloux (1967) experimentally investigated crack growth in different classes of aluminum alloys under various load spectra. By means of electron fractography they observed the striation patterns under predefined variable amplitude loading with: (a) different stress range levels with a constant maximum stress, (b) constant stress range with different levels of maximum stress, (c) a

programmed pseudo-random variable amplitude loading spectrum, and (d) a uniform constant amplitude loading spectrum with single overloads and underloads. Tests were conducted on center notched specimens and the fatigue striations were observed. The results of this study concluded that growth of a fatigue crack occurs only during a stress rise potion in a cycle. It was also observed that under pseudo-random loads with variable maximum stress, the sequence of loads greatly influences the crack growth rate. Their experimental results have since served as a basis for comparison of crack growth models developed in literature.

Lu and Liu (2010) developed a new formulation of crack growth which is principally different from classical reversal-based approaches. It is based on incremental crack growth at any time within a cycle. Based on their approach, fatigue analysis can be performed at various time and length scales without cycle counting. Since their method studies the instantaneous stress state, the stress ratio effect is inherently considered in the crack growth analysis. The authors adopt the reverse plastic zone concept to determine the lower integration limit for the time integral to calculate the crack length under both constant and variable amplitude loading. The model was validated with experimental data for different metallic materials under various loading spectra and showed good agreement with experimental results.

Experimental Work on Fatigue Crack Growth in Stiffened Panels

Nussbaumer et. al. (1999) studied the propagation of long fatigue cracks in complex welded box beams under constant-amplitude loading. The specimens were fabricated to simulate the cellular structure of a stiffened double ship hull. Ten specimens were tested under four-point bending employing a load control test setup. The specimens were tested under positive load ratio and it was observed that the crack growth followed a four-stage propagation scheme as outlined in Table 1 and Figure 4.

Table 1 - Four stage crack propagation scheme in box-beam specimens (Nussbaumer et. al., 1999)

Crack Growth Stage	Observation
Stage I	Crack initiates and grows into a through-thickness crack
Stage II	Through-thickness crack grows into the adjacent cell
Stage III	Crack reaches the web and flange intersection, becoming a four-ended crack
Stage IV	Crack propagation through the remaining part of the flange

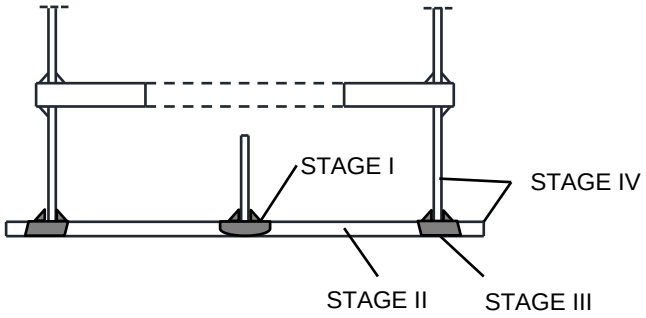

Figure 4 – Locations of the four stages of crack propagation (Nussbaumer et. al., 1999)

The study concluded that the box specimens showed remarkable resistance to unstable crack growth owing to the inherent redundancy of the cellular structure and the high fracture toughness of the A710 steel. It was also observed that crack propagation rate depends greatly on the applied stress range and the residual stress field in the panel. Nussbaumer et. al. (1999) developed a finite element model which employed the modified crack closure concept (Rybicki and Kanninen, 1977) and J-integral (Rice, 1968) to determine stress intensity factors.

Dexter and Pilarski (2002) extended the work done by Nussbaumer et. al. and conducted experiments to study crack growth in welded stiffened panels, that were fabricated into large box-beams. Ten specimens were tested under a four-point bending test setup, with varying material specifications, stiffener geometry and crack plane detail. The crack was initiated with a saw cut in

the middle and allowed to propagate under cyclic loading. Table 2 shows the test matrix for the tested specimens.

Table 2 - Test matrix for specimens tested under four-point bending

Specimen	**Type of steel**	**Type of stiffener**	**Stress range (MPa)**	**Notch length (2a) (mm)**	**Detail on crack plane**
Baseline	ASTM A572 Gr. 50	No stiffener	33	204	None
A-1	ASTM A572 Gr. 50	3x4x3/8 angle	42	400	Solid stiffener
A-2	ASTM A572 Gr. 50	3x4x3/8 angle	42	280	Access hole
A-3	ASTM A572 Gr. 50	3x4x3/8 angle	42	350	Raised drain hole
A-4	ASTM A572 Gr. 50	3x4x3/8 angle	42	200	Butt weld/access hole
A-2a	ASTM A572 Gr. 50	3x4x3/8 angle	42	100 and 200	Multiple notches access holes
T-1	ASTM DH-36	4x4x5# tee	42	360	Solid stiffener
T-2	ASTM DH-36	4x4x5# tee	42	200	Butt/weld access hole
T-3	ASTM DH-36	4x4x5# tee	46	460	Solid stiffener
T-4	ASTM DH-36	4x4x5# tee	46	440	Butt/weld access hole

The study concluded that the presence of compressive residual stresses between the stiffeners retards the crack propagation rate and that the type of steel has no significant impact of crack growth rate. Variations in stiffener geometry and stiffener cutouts were shown to have little effect on the crack growth rate. However, the presence of a transverse butt-weld eliminated the restraining effect of the longitudinal stiffeners and the crack propagation rate was similar to that in a plate with no stiffeners. Dexter et. al. (2003) used these test results to develop an analytical

model that predicts the crack growth in a panel with multiple welded stiffeners. Their model was based on the existing study proposed by Nussbaumer (1993). This model includes the effects of stiffener restraint, severed stiffeners and residual stresses to predict crack growth in a stiffened panel with a center through crack and multiple welded stiffeners. A finite element model was developed to determine the effective stress intensity factor. Residual stresses were incorporated into the model as thermal stresses. The finite element showed good agreement with the results of the analytical model. Crack growth curves were established for different conditions (e.g. no residual stresses, no geometry factors) to understand the effect of each factor. It was observed that residual stresses had the greatest impact on the rate of crack growth.

In another expansion to the scope of the study, Mahmoud and Dexter (2005) studied the crack growth behavior in stiffened panels under axial tension loading. Five specimens with varying stiffener spacing, heat inputs for welding, stiffeners type and plate thickness were tested under a load controlled leveraging test setup. Measurements for residual stresses were made by employing the coupon sectioning method (Konda and Ostapenko, 1964) as it the most economical and accurate method available (Mahmoud and Dexter, 2005). The test matrix for their experimental work is shown in Table 3.

Table 3 - Test matrix for specimens tested under tensile loading

Specimen #	**Plate thickness (mm)**	**Type of stiffener**	**Stiffener spacing (mm)**	**Heat input**
S1	13	Bulb tee	381	Medium
S2	13	Bulb tee	381	High
S3	13	Bulb tee	305	Medium
S4	13	101 x 76 x 8 angle	381	Medium
S5	9	Bulb tee	381	Medium

It was observed that the crack growth remained stable throughout the testing procedure as observed in the previous studies. It was also concluded that the crack growth retardation occurred due to two main effects: the residual stresses and the stiffener restraint. As the stiffener spacing decreases, the magnitude of the compressive residual stress increases and thus retards crack growth. A finite element model was also developed and static analysis was conducted at various crack sizes to determine the J-integral values. Faulkner's residual stress model (Faulkner, 1975) was used to incorporate residual stresses into the model. A parametric finite element analysis was performed to determine the best combination for the value of C and residual stresses to match the actual crack growth behavior of the specimens.

Probabilistic Fatigue Crack Growth Analysis

Mahmoud et. al. (2014) conducted probabilistic crack growth analysis to determine the effect of randomness in material parameters C and m on the fatigue reliability of stiffened panels. The study concluded that crack growth parameter C causes a large scatter in the crack growth profile and the corresponding number of cycles to failure. The crack growth rate was also observed to decrease in the regions between the stiffeners due to the presence of compressive residual forces. The threshold stress intensity factor of the material had the largest impact on the number of cycles to failure. It was observed that increasing the value of the threshold stress intensity factor by 50 MPa resulted in an increase in the number of cycles to failure by over 5 times. However, this study did not include the critical crack size in formulating the probabilistic model.

Xiao et. al. (2006) employed LEFM to study the fatigue life of the ribs in a steel orthotropic deck with different depths of weld penetration in butt welded joints of Kinuura Bridge. Using stress data from structural health monitoring and by incorporating relevant geometry factors, the fatigue life of longitudinal ribs was determined using LEFM for incomplete weld penetration depths ranging from 0.1 to 4 mm. The study concluded that large volume of truck traffic also contributed

to low fatigue life of longitudinal ribs. Furthermore, incomplete weld penetration depths above 3 mm can significantly reduce fatigue life. The cores drilled across the cracked welds confirmed that fatigue cracks develop from incomplete penetration of 2 to 3 mm. Zhao et. al. (1994) compared the reliability over time of full penetration butt welds in a steel bridge subjected to fatigue loading using LEFM and AASHTO S-N approach. The study concluded that LEFM is a powerful alternative to the AASHTO S-N curve approach for determining reliability, since it can be updated with crack information as it becomes available through inspections. Cheung and Li (2003) performed probabilistic analysis of a steel girder bridge with flange cover plates using LEFM approach by incorporating finite strip analysis method. The study concluded that fatigue reliability of the bridge can be significantly improved by extending the cover plates to the full span of the bridge. Kim et. al. (2013) established optimum inspection and maintenance schedules based on LEFM of fatigue critical details in a ship structures by maximizing the service life and minimizing the expected life-cycle costs using a decision tree model approach. Finally, Soliman et. al. (2013) utilized stochastic LEFM as well to establish the optimum inspection schedules for bridges, with multiple fatigue critical details.

Although the above studies determined the time variant reliability of structures with complex geometries considering loads and material properties as random parameters, the critical crack size was determined without performing detailed analysis. Furthermore, the nature of the failure was not determined (i.e. ductile or brittle). In this study, the critical crack size will be determined by using a failure assessment diagram analysis. Additionally, probabilistic fatigue analysis of complex geometries can be computationally expensive, and in some cases impractical, due to the large computational demand. Deep learning will be implemented in this thesis to reduce the computational time associated with probabilistic analysis.

CHAPTER II

METHODOLOGY

Crack Propagation in Stiffened Panels

In order to quantify the crack growth in a panel with welded longitudinal stiffeners, this study adopts the model proposed by Dexter et. al (2003). This model was developed to study the crack growth behavior in stiffened ship hulls considering the effect of longitudinal stiffeners and the residual stresses. For this type of structures, the ends of the member have to deform in a way that is compatible with the nearby members. Therefore, a cracked member surrounded by uncracked members will experience a decrease in the stress range. This phenomenon is called load shedding, which contributes to the decrease in crack growth rate. Dexter et. al. (2003) formulated an analytical model that can determine the modified stress intensity factor for a stiffened plate, calculated by superimposing the effects of stiffener restraint K_1, effects of severed stiffeners K_2 and the residual stresses K_{res}. Figure 5 shows the stress intensity factor components that are superimposed to establish the final value of K. Formulation of these components is explained in the subsequent sections.

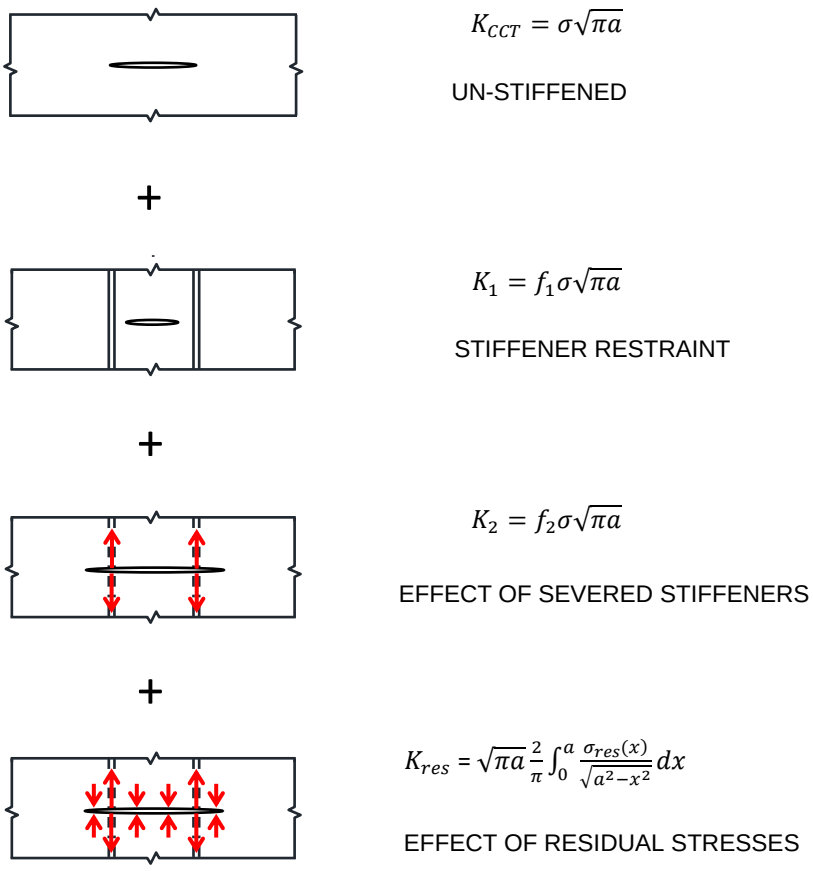

Fig. 5 - Overview of components of superposition

Effect of Stiffener Restraint

Isida (1973) studied the effect of stiffeners on the crack growth and developed a stress intensity factor for a plate with stiffened edges. Nussbaumer (1994) examined Isida's solution and noticed that it overestimates the restraining effects of the stiffeners. Nussbaumer then calibrated Isida's solution to fit Poe's results (Poe, 1971), who studied crack propagation in riveted plates, by calibrating model parameters α_1 and α_2. Nussbaumer (1994) formulated the solution for stiffener restraint as

$$f_1 = \left(1 - \frac{1}{f_{k,i}}\right)\left(\frac{1}{1+\beta_i}\right)^{\alpha_1} + \frac{1}{f_{k,i}} + \frac{0.3\chi_i^2}{f_{k,i}}\left(\frac{4}{\beta_i^2 - 2\beta_i + 4} - 1\right) - 1 - \alpha_2\left(\frac{\chi_i^{10} + \chi_i^{30} + \chi_i^{50}}{f_{k,i}}\right)\left(\frac{4}{\beta_i^2 - 2\beta + 4} + 1\right)$$

for $\chi \leq 0.95$ Eq. (5)

where a is half the crack size, $\chi_i = \frac{a}{x_i}$, $\beta_i = \frac{A_{st,i}}{t_{pl} x_i}$, x_i is the distance from the center of the crack to the i^{th} stiffener, $A_{st,i}$ is the cross-sectional area of the i'th stiffener, $\alpha_1 = 1$, $\alpha_2 = 0.1$ and $f_k = \frac{1 - 0.5\chi + 0.326\chi^2}{\sqrt{1-\chi}}$, which is the finite width correction factor. The total stiffener restraint coefficient can then be found by summing the restraint effects for individual stiffeners.

$$f_1 = \Sigma f_{1,i} \quad \text{Eq. (6)}$$

It should be noted that Eq. (5) is valid only for $\chi_i \leq 0.95$. It does not allow the crack to grow into the stiffener. Linear interpolation will be used to account for crack propagation through the stiffeners as explained in the next section.

Effect of Severed Stiffeners

The effect of severed stiffeners is addressed by incorporating the factor, f_2, which models the stiffeners as point forces F acting on the crack surface. These forces represent tension that the stiffener was carrying when it was intact.

The splitting force F is (Dexter and Pilarski, 2002):

$$F = \sigma\left(\frac{\mu}{1-\mu}\right) \cdot \left(A_{pl}\right) \quad \text{Eq. (7)}$$

where $\mu = \frac{A_{st}}{A_{st} + A_{pl}}$, A_{st} is the area of the stiffener and A_{pl} is the area of the plate.

These forces cause an increase in the stress intensity factor, which is calculated as (Dexter and Pilarski, 2002)

$$K = \frac{2F}{t_{pl}\sqrt{\pi a}} \cdot \frac{a}{\sqrt{a^2 - s^2}} \qquad \text{Eq. (8)}$$

where t_{pl} is the thickness of the plate, a is half crack size and s is half stiffener spacing.

Using the same crack length and the inclusion of the generic terms χ_i and μ, Equation (8) can be converted into a correction factor f_2 as (Dexter and Pilarski, 2002)

$$f_{2,i} = \frac{2\mu}{\pi(1-\mu)} \cdot \frac{{}^{2s}/_{x_i}}{\sqrt{\chi_i^2 - 1}} \qquad \text{for } \chi_i > 1 \qquad \text{Eq. (9)}$$

where x_i is the distance to the i^{th} severed stiffener and χ_i is the normalized distance to the i^{th} severed stiffener.

The Stiffened Panel Coefficient

Now that the formulations of f_1 and f_2 have been established, the stiffened panel coefficient can be formulated by superposition to obtain the complete coefficient for crack growth as (Dexter and Pilarski, 2002)

$$f_{st} = 1 + \Sigma f_{1,i} + \Sigma f_{2,i} \qquad \text{Eq. (10)}$$

where 1 represents the unstiffened plate (i.e., K_{CCT} in Figure 5).

A sudden increase in the coefficient is observed at the location of the stiffeners due to the assumption that the stiffener is immediately severed as the crack reaches it. However, experimental results (Dexter and Pilarski, 2002) have shown that the crack grows through the stiffener in a manner similar to that of the plate. Therefore, linear interpolation between the un-

severed and severed stiffener can be performed to obtain a more reasonable and realistic variation of the coefficient through the stiffener (Dexter et al., 2003). The first point of interpolation is the last accurate point that f_1 is valid for. The second interpolation point can be located at a point equal to radius of the crack face from the centerline of the stiffener. This formulation was developed by Poe (Poe, 1971) and is shown schematically in Figure 6 (Dexter, 2003).

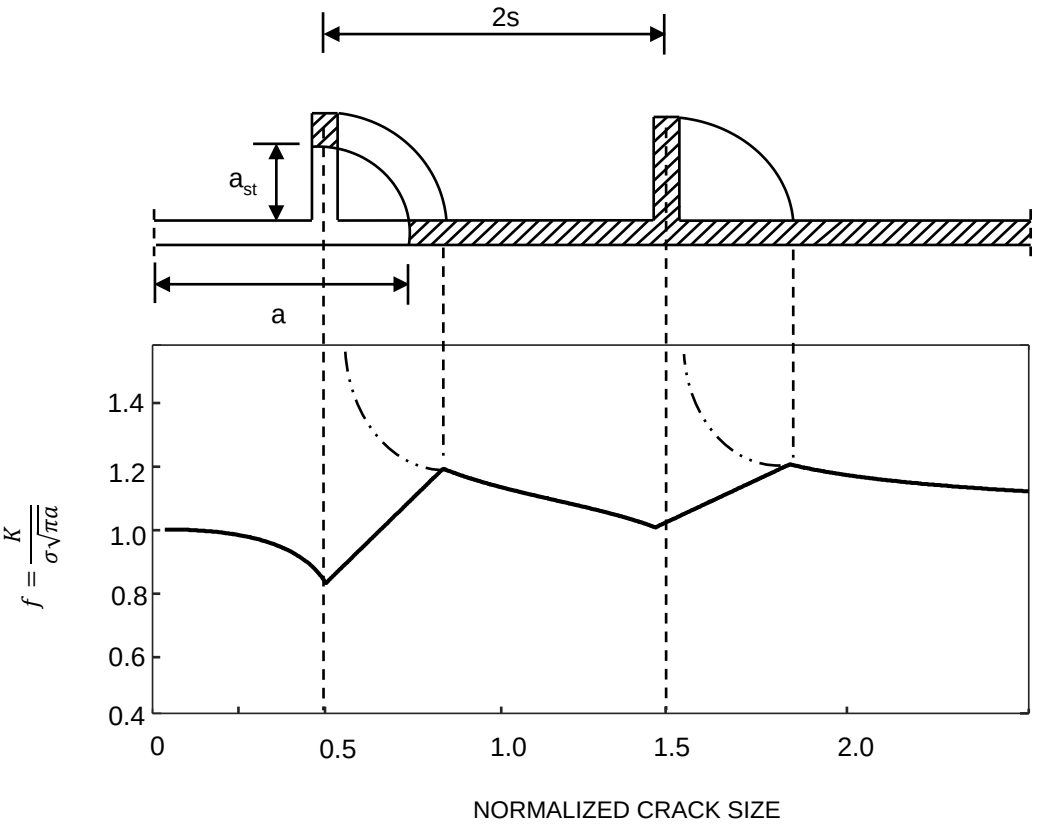

Fig. 6 - Linear interpolation across severed stiffener (adapted from Nussbaumer, 1994)

Residual Stresses and Residual Stress Intensity Factor

Residual stresses have a considerable effect on the crack growth in welded structures (Mahmoud and Dexter, 2005). The presence of compressive residual stresses can reduce the crack growth rate considerably while high tensile residual stresses may not affect the crack growth rate

(Mahmoud and Dexter, 2005). Therefore, residual stresses need to be accounted for when calculating the stress intensity factor.

Tests were conducted by Kondo and Ostapenko (1964) to measure the residual stresses in a stiffened panel, where they used a carefully refined coupon pattern to accurately capture the residual stress field along the panel (Kondo and Ostapenko, 1964). It was observed that the welding process results in high tensile residual stresses in the vicinity of the stiffener and compressive residual stresses in the region between stiffeners.

However, it was observed by Dexter and Pilarski (2002), that the measured residual stresses do not satisfy equilibrium. This was attributed to errors in measurement and coupon cutting procedures (Dexter and Pilarski, 2002). The idealized distribution of the residual stress used herein is based on the model adopted by Dexter and Pilarski (2002). This model defines the tensile regions around the stiffeners as triangles with a base width proportional to the plate thickness. The half width of this triangular region can be taken as 3.5 times the thickness of the plate (Dexter and Pilarski, 2002). The maximum value of the tensile residual stress is assumed to be equal to the yield strength of the plate material at the location of the stiffener. Figure 7 shows the residual stress distribution in a stiffened panel adopted in this study. To quantify the residual stress intensity factor, Greene's function is integrated over the crack length. Greene's function (Rooke and Cartwright, 1976) models the stress intensity factor for symmetric splitting forces acting on the crack. This yields the residual stress intensity factor along the stiffened panel as

$$K_{res} = \sqrt{\pi a}\,\frac{2}{\pi}\int_0^a \frac{\sigma_{res}(x)}{\sqrt{a^2-x^2}}\,dx \qquad \text{Eq. (11)}$$

To formulate the stiffened panel stress intensity factor, the effect of stiffener restraint, stiffener separation and the residual stresses will be superimposed as shown in Figure 5. Finally, the range of effective stress intensity factor is determined as illustrated in Figure 8 (Dexter and Pilarski, 2000).

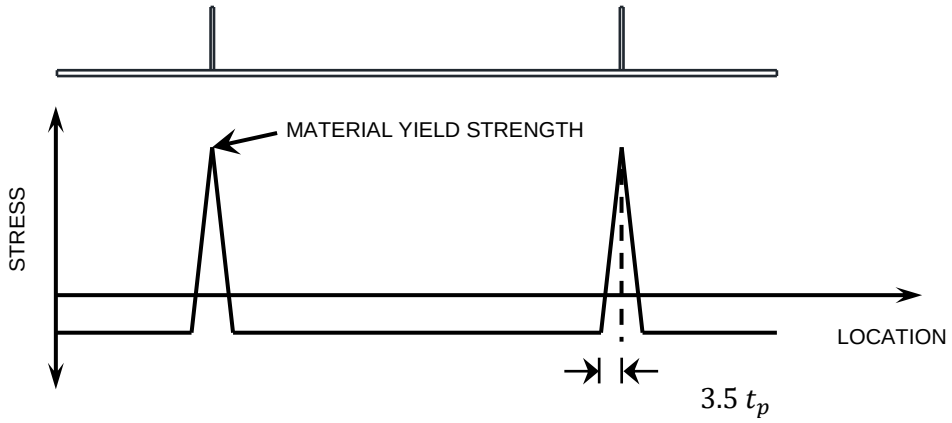

Fig. 7- Residual stress distribution along a stiffened panel

The total stress intensity factor K_{total} is a sum of applied stress intensity factor $K_{applied}$ and the residual stress intensity factor $K_{residual}$. $K_{applied}$ can be split into $K_{applied,max}$, $K_{applied,min}$, and $K_{applied,op}$, corresponding to the maximum and minimum applied stresses, and the crack opening stress. These components are added to $K_{residual}$ individually to determine the total stress intensity factor at the respective points in the load cycle. Under progressive loading, equilibrium is reached when the crack surfaces start to separate at the crack front. Therefore, it can be assumed that the sum of the stresses at this point is zero and the total stress intensity factor at this point, $K_{applied,op} = 0$. The resulting expression is $K_{applied,op} = -K_{residual}$. If $K_{applied,min}$ is less than the $K_{applied,op}$, there will be crack closure and $\Delta K_{eff} = K_{applied,max} - K_{applied,op}$. If $K_{applied,min}$ is greater than $K_{applied,op}$, there will be no crack closure and $\Delta K_{eff} = K_{applied,max} - K_{applied,min}$.

Failure Assessment Diagrams

As a crack grows through a member, it may eventually reach a critical size, after which sudden fracture failure may occur. In prior studies (Kwon et al., 2012, Zhao et al., 1994a, Cheung and Li,

2003), this crack size is assumed on basis of the engineering judgement or taken as the maximum dimension available for the crack to grow. Failure Assessment Diagram (FAD) is a type of interaction diagram which can be used to determine whether the structure is safe or not, given a certain crack size. The vertical axis in a FAD represents a measure of the applied stress conditions required to cause sudden fracture and the horizontal axis represents the applied load required to cause plastic collapse. An assessment line is plotted in accordance with type of failure diagram to represent the capacity. Finally, calculations for a given flaw will result in a set of coordinates on the FAD. The location of this point can be compared to the assessment line to determine whether the flaw is acceptable or not. A point that lies in the region bounded by the assessment line is considered acceptable and a point that lies outside the bounded region is considered unacceptable.

Several studies in literature integrate the FAD with probabilistic fatigue analysis. Zhao et. al. (1997) considered the uncertainty in the stress intensity factor and conducted stochastic analysis covering the parameters in the FAD analysis. However, this study did not consider the uncertainty associated with assessment points. Wang et. al. (1999) used a similar approach and developed a probability density function of the safety factor n, by considering uncertainty in crack detection and material properties. Both approaches did not consider the uncertainty in the applied loads. In this thesis attempts are made to conduct the time variant flaw assessment considering uncertainty in the applied loads in addition to those associated with material properties to determine the Probability Distribution Function (PDF) of the critical crack size. This PDF is used in the performance function to determine the failure probability.

FAD has three options for assessment outlined in the British Standard BS 7910 (BSI, 2013) namely Options 1, 2 and 3. Option 1 is suitable for cases where detailed stress-strain data is not available. Option 2 requires true uniaxial stress-strain data of the material while Option 3 requires detailed information on material, loading and geometry, and uses both elastic and elastic-plastic

analyses of the structure, which may require the use of detailed finite element modelling. In this study, Option 1 be used.

Assessment Option 1 (BSI, 2013)

This assessment option can be utilized when limited information on the material properties or the external forces is given. It does not require a detailed stress-strain data for the material. No inherent safety factors are included, resulting in a realistic assessment that is suitable for stochastic analysis. The assessment point has the coordinates (L_r, K_r) where L_r is the load ratio defined as

$$L_r = \frac{\sigma_{ref}}{\sigma_Y} \quad \text{Eq. (12)}$$

in which σ_{ref} is calculated using an appropriate reference stress solution from Annex P of BS 7910 (2013) and σ_Y is the yield strength of the material. K_r is the fracture ratio defined by Equation (13) or Equation (14).

$$K_r = \frac{K_I^p + VK_I^s}{K_{mat}} \quad \text{Eq. (13)}$$

$$K_r = \frac{K_I^p + K_I^s}{K_{mat}} + \rho \quad \text{Eq. (14)}$$

where K_I^p is the primary applied stress intensity factor having the general form presented by Equation (1), K_I^s is the stress intensity factor developed due to secondary stresses, V is the plasticity correction factor, ρ is the plasticity interaction factor and K_{mat} is the fracture toughness of the material.

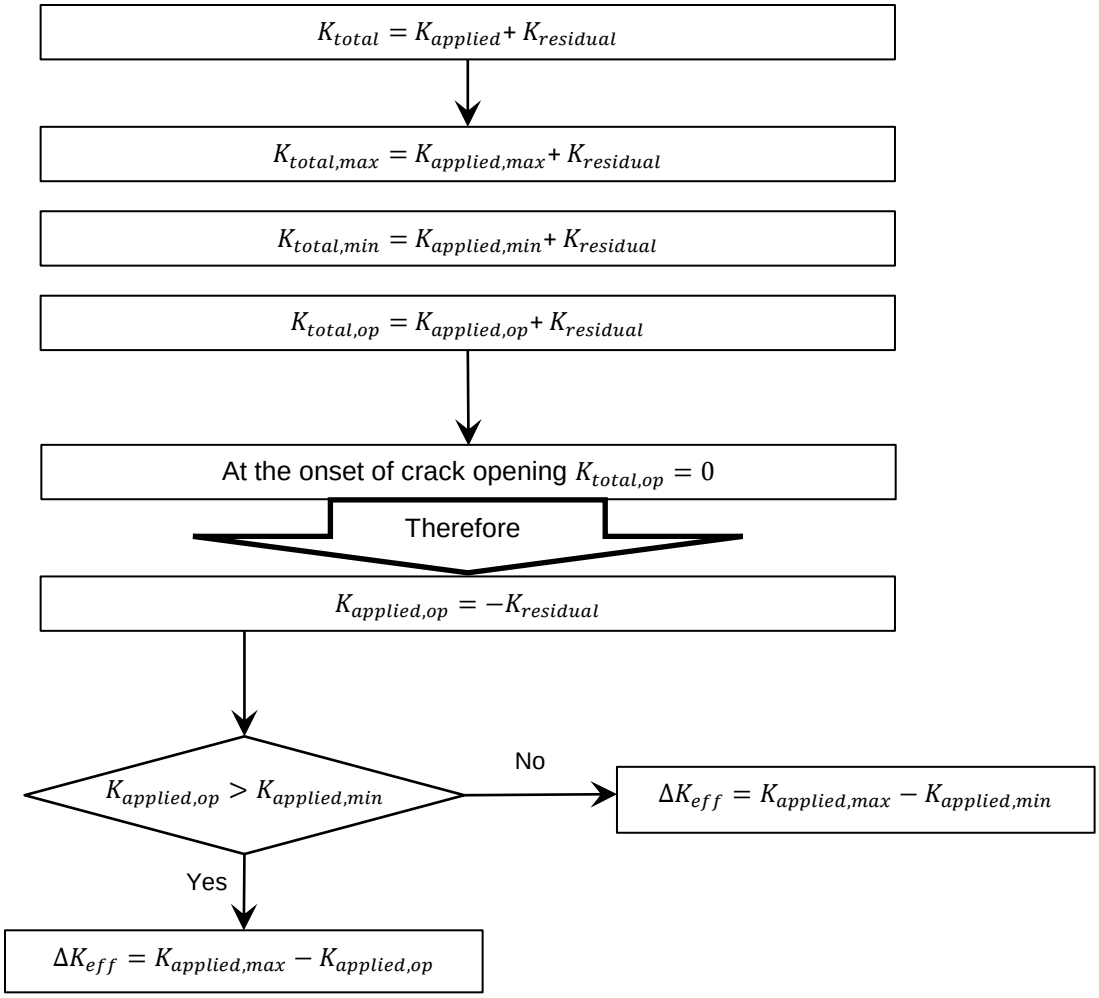

Fig. 8 - Procedure for determining the effective stress intensity factor range

The plasticity effects can be ignored for this study since the applied loads and stress ranges are very low, resulting in negligible plasticity effects (Dexter and Pilarski, 2000). Hence, the equation can be reduced to

$$K_r = \frac{K_I}{K_{mat}} \qquad \text{Eq. (15)}$$

where K_I includes both primary and secondary applied stress intensity factors.

The assessment line for Option 1 is defined as (BSI, 2013)

$$f(L_r) = \begin{cases} \left(1 + \frac{1}{2}L_r^2\right)^{-0.5}\left\{0.3 + 0.7e^{(-\mu L_r^6)}\right\} & for\ L_r \leq 1 \\ f(1)L_r^{(N-1)/2N} & for\ 1 < L_r < L_{r,max} \\ 0 & for\ L_r \geq L_{r,max} \end{cases} \quad \text{Eq. (16)}$$

where $\mu = min\left(0.001\frac{E}{\sigma_Y}, 0.6\right)$, $N = 0.3\left(1 - \frac{\sigma_Y}{\sigma_u}\right)$ and $L_{r,max}$ is the maximum cut-off value for L_r to prevent local plastic collapse and is calculated as

$$L_{r,max} = \frac{\sigma_Y + \sigma_u}{2\sigma_Y} \quad \text{Eq. (17)}$$

where σ_Y is the yield strength and σ_u is the ultimate tensile strength of the material.

Equation (17) is applicable to materials that do not exhibit yield discontinuity. For material that exhibit a yield discontinuity, the assessment line is described as (BSI, 2013)

$$f(L_r) = \begin{cases} \left(1 + \frac{1}{2}L_r^2\right)^{-0.5} & for\ L_r \leq 1 \\ \left(\lambda + \frac{1}{2\lambda}\right)^{-0.5} & L_r = 1 \\ f(1)L_r^{(N-1)/2N} & for\ 1 < L_r < L_{r,max} \\ 0 & for\ L_r \geq L_{r,max} \end{cases} \quad \text{Eq. (18)}$$

where the quantity $\lambda > 1$ is defined as

$$\lambda = 1 + \frac{E\Delta\varepsilon}{R_{eL}} \quad \text{Eq. (19)}$$

in which E is the modulus of elasticity, $\Delta\varepsilon$ is the change in strain at yield stress without an increase in stress and R_{eL} is the yield strength of the material.

If the assessment point lies in the region bounded by the assessment line and the axes, the flaw is considered acceptable. If it lies outside the bounded region, it is considered unacceptable. A typical Option 1 FAD is shown in Figure 9, where assessment point A represents an unacceptable flaw and point B represents an acceptable flaw. The area under the assessment line is divided into three zones as shown in Figure 8. If the assessment point lies in Zone 1, the failure tends to be

fracture controlled. If it lies in Zone 2, the failure tends to be a mixed mode failure. If the assessment point lies in Zone 3, the failure tends to be more ductile.

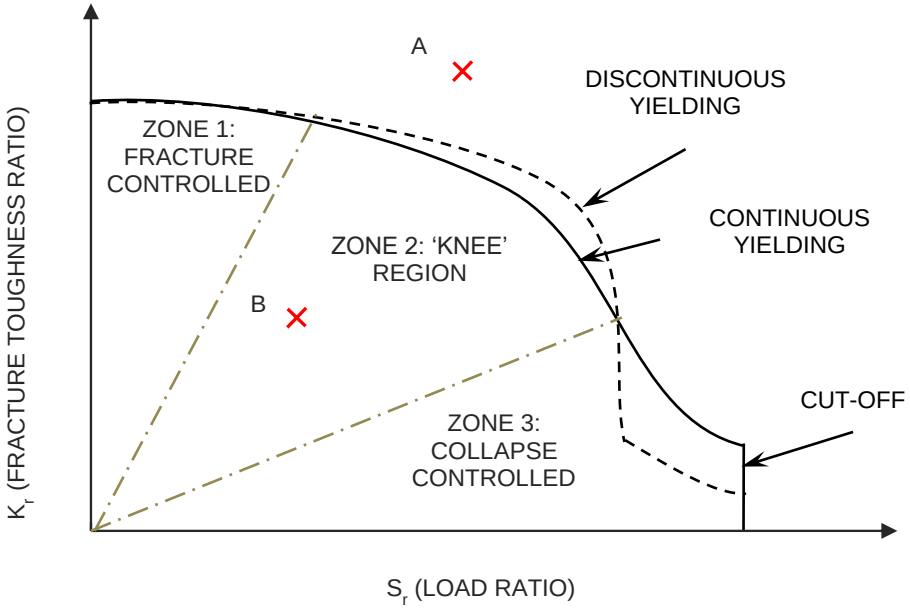

Fig. 9 - Typical Option 1 FAD

System Performance and Time Dependent Reliability Analysis

Due to the uncertainties present in loads and material properties, probabilistic analysis is essential in understanding the fatigue performance of the structure over time. By modelling the uncertainty in loads and material properties, a probabilistic crack growth profile can be established using Monte Carlo simulation. The probabilistic distribution parameters of the crack size at an instant in time can then be determined using MATLAB distribution fitting toolbox. Propagating cracks eventually reach a critical size, which is determined using FAD analysis. Next, the probability of failure can be determined using the performance function

$$g(X,t) = a_{cr}(X) - a(X,t) \qquad \text{Eq. (20)}$$

Where X is the vector of random variables governing the problem, a_{cr} is the critical crack size and $a(t)$ is the crack size at time t.

The probabilistic distribution of the critical crack size is established through probabilistic time variant FAD analysis. MATLAB Distribution fitting toolbox is used to determine the probabilistic descriptors of the critical crack size. Random samples of the critical crack size and the instantaneous crack size are drawn next using MATLAB random number generator and Monte Carlo simulation is performed to determine the time variant probability of failure as

$$P_f(t) = P[g(X,t) \leq 0] \quad \text{Eq. (21)}$$

where $P_f(t)$ is the probability of failure at time t.

Next the time variant reliability index is determined as

$$\beta(t) = \Phi^{-1}\left[1 - P_f(t)\right] \quad \text{Eq. (22)}$$

where $\beta(t)$ is the reliability index at time t and Φ is the cumulative density function (CDF) of the standard normal distribution.

In this study, the applied stresses σ_{max} and σ_{min}, crack growth parameter C, the yield strength σ_Y and the ultimate tensile strength σ_u are considered as random variables. Figure 10 shows schematically, the probability distribution of the crack size at different times along the service life and the probability distribution of the critical crack size.

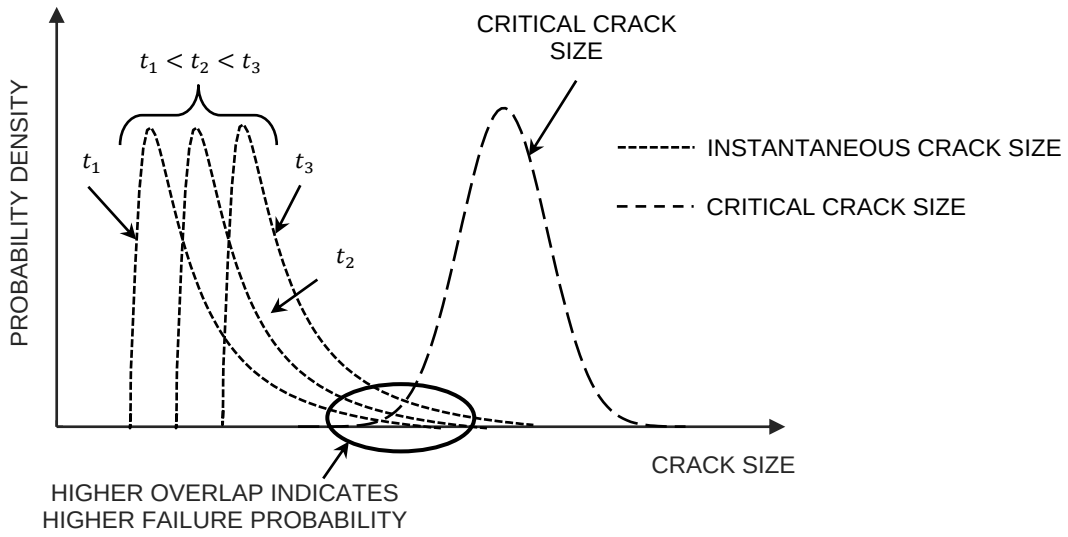

Fig. 10 – A schematic representing the probabilistic distributions of instantaneous crack size and critical crack size

Machine Learning and Deep Learning

Over the past few decades, the exponential progress in the development of higher performance Central Processing Units (CPUs) and Graphics Processing Units (GPUs) has paved the road to apply machine learning in solving complex computational tasks in various scientific fields. Machine learning and deep learning algorithms have the ability to recognize patterns, classify data, recognize images, sounds and make predictions. The exceptional ability of machine learning to develop nonlinear approximations, its multi-variate learning ability and its flexibility, have made it a useful tool for engineering applications. It employs a series of algorithms used in data driven systems, such as genetic algorithms, support vector machines, artificial neural networks and neural-fuzzy systems. Since machine learning is capable of modelling internal connections and tendencies in a complicated set of data, it can be used for fatigue assessment of deteriorating structures.

Zio et. al. (2012) used a Bayesian-based relevance vector machine (RVM) to model the remaining useful life of a component or structure based on data collected under fatigue deterioration. The

RVM learning procedure utilized the sparse data available for degradation trajectory and extrapolated the results to determine the remaining useful life. The obtained results were proven satisfactory in terms of accuracy and computational run time. Mohanty et. al. (2015) adopted a genetic programming approach for predicting the fatigue crack growth on an aluminum specimen subjected to constant amplitude loading and demonstrated its superiority compared to an artificial neural network. Zhao et. al. (2106) used a radial based artificial neural network to predict the crack growth in a steel specimen with a center crack. The predictions of the neural network demonstrated good agreement with experimental results. Furthermore, Stern et. al. (2017) developed a machine learning based surrogate model by implementing a support vector machine and a logistic regression technique, to reduce the runtime required to perform Monte Carlo simulation on a gas distribution network after an earthquake. In this study a deep learning approach is proposed to reduce the time and computational cost encountered while performing Monte Carlo simulation.

Deep learning is a branch of machine learning which can be used to employ various hidden layers of neural networks to interpret features and relationships directly from a large set of unlabeled data. A typical deep neural network is shown in Figure 11. Neural networks are composed of three types of layers, input, hidden, and output layers. Input layer is responsible for feeding the input parameters into hidden layers. Each hidden layer consists of several neurons, in each neuron, the input units are converted to nonlinear functions of linear combinations of assigned weights and bias values. Using the assigned weights and bias values, the neural network algorithm can optimize the results and train the network to minimize the bias values with respect to expected outputs. A deep learning neural network is trained by evaluating and minimizing the error between the predicted value and the actual value using back propagation or feed forward approaches. The training consists of three parts; (a) training, where the neural network is trained by fitting mathematical models to data, (b) testing, where the error is evaluated for the trained

model, and (c) verification, where the final best fit model is used to predict and compare the results based on the model selected during testing. Many deep learning frameworks such as Keras (Ketkar, 2017), Tensorflow (Abadi et. al., 2016), Theano (Al-Rfou et al., 2016) and Caffe (Jia et al., 2014), are available as open source software packages. For this study, tensorflow is used.

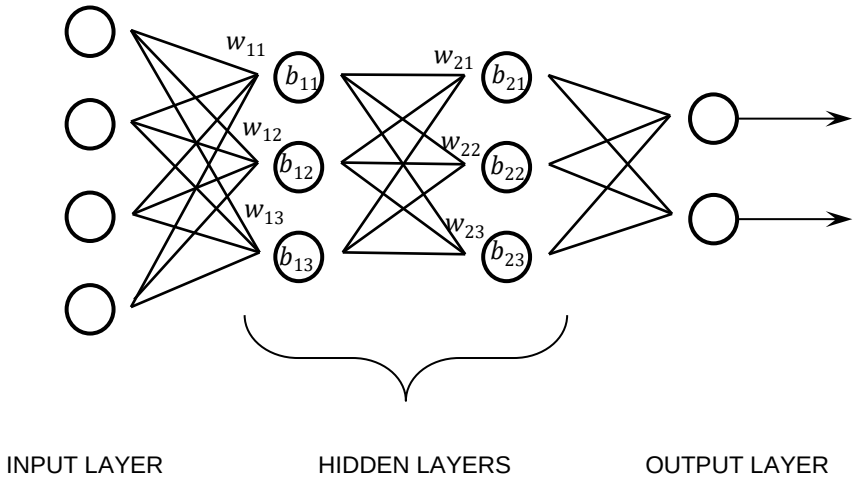

Fig. 11 - A typical neural network employed in a deep learning framework

Tensorflow is an open source deep learning engine developed by Google. Owing to its flexibility and versatility, it can be easily utilized for applications in engineering research. TensorFlow gives its users the ability to select the type of neural network that can be built into the deep learning dataflow graph. Some examples include Convolutional Neural Networks (LeCun et al., 2015), Recurrent Neural Network (LeCun et al., 2015) and Recursive Neural Network (Socher et al., 2011). TensorFlow uses a single dataflow graph to perform computations throughout its algorithms. This graph contains several vertical nodes and edges. Each vertex represents a unit of local computation and each edge represent the input or output routs to or from the vertices. The computations at vertices and the multi-dimensional matrices of values flow along the edges are referred to as operations and tensors, respectively. A typical TensorFlow dataflow graph contains several subgraphs that are connected through shared variables and queues. The execution process

of the graph starts with one or more edges to feed the input tensors into the dataflow. The reader module then takes a reference handle (r) and produces the value of the variable (state[r]) as a dense tensor. Shuffle queue is then responsible for extracting randomized batch data from the reader and pass it to the preprocessing unit that transforms the input records (e.g., decodes images and applies random distortions) concurrently. Next, the input queue is responsible for producing data batches and feeding the core training subgraph. Finally, the input batches and a set of model parameters are analyzed through many concurrent steps of the training subgraph. The training process also involves saving and restoring data into/from a distributed file system, applying gradient updates, and running periodic checkpoints for fault tolerance. A typical TensorFlow dataflow graph for training is presented in Figure 12 (Abadi et al., 2016). Raw unlabeled data is fed into the input layer which reads this data. It is then shuffled and organized into tensors and fed into the neural network for training, where weights and biases are initialized for each neuron. A cost function determines the amount of error after each iteration and an optimizer function computes the gradients which determine the calibration of the weights and biases. This process can be repeated until the MSE is minimized to the desired value.

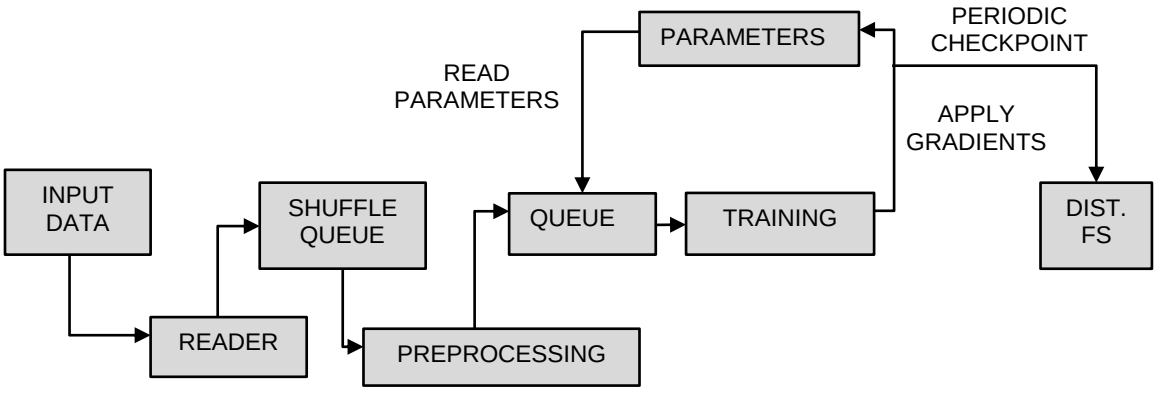

Fig. 12 - Dataflow graph for TensorFlow

Probabilistic Fatigue Assessment Framework

A probabilistic framework for fatigue assessment of stiffened structures is established in this study. Figure 13 shows the different modules of the framework First, a finite element model is developed to determine stresses at the crack location under applied loads. Next, a crack growth model capable of quantifying the crack growth through a stiffened plate is used to model the crack growth behavior under cyclic loading. Considering uncertainties in the applied loads and the material properties, Monte Carlo simulation is conducted to determine the probabilistic crack growth. This data set for crack growth is then used to train a deep learning framework to generate a larger number of samples for probabilistic crack growth. Using the deep learning-based probabilistic crack growth, crack size distribution is determined at different times along the service life. Next, probabilistic failure assessment curve is plotted to determine the probabilistic distribution of the critical crack size considering uncertainties in loads and material properties. Finally, the time variant probability of failure and reliability index are determined through the results of simulating the performance function.

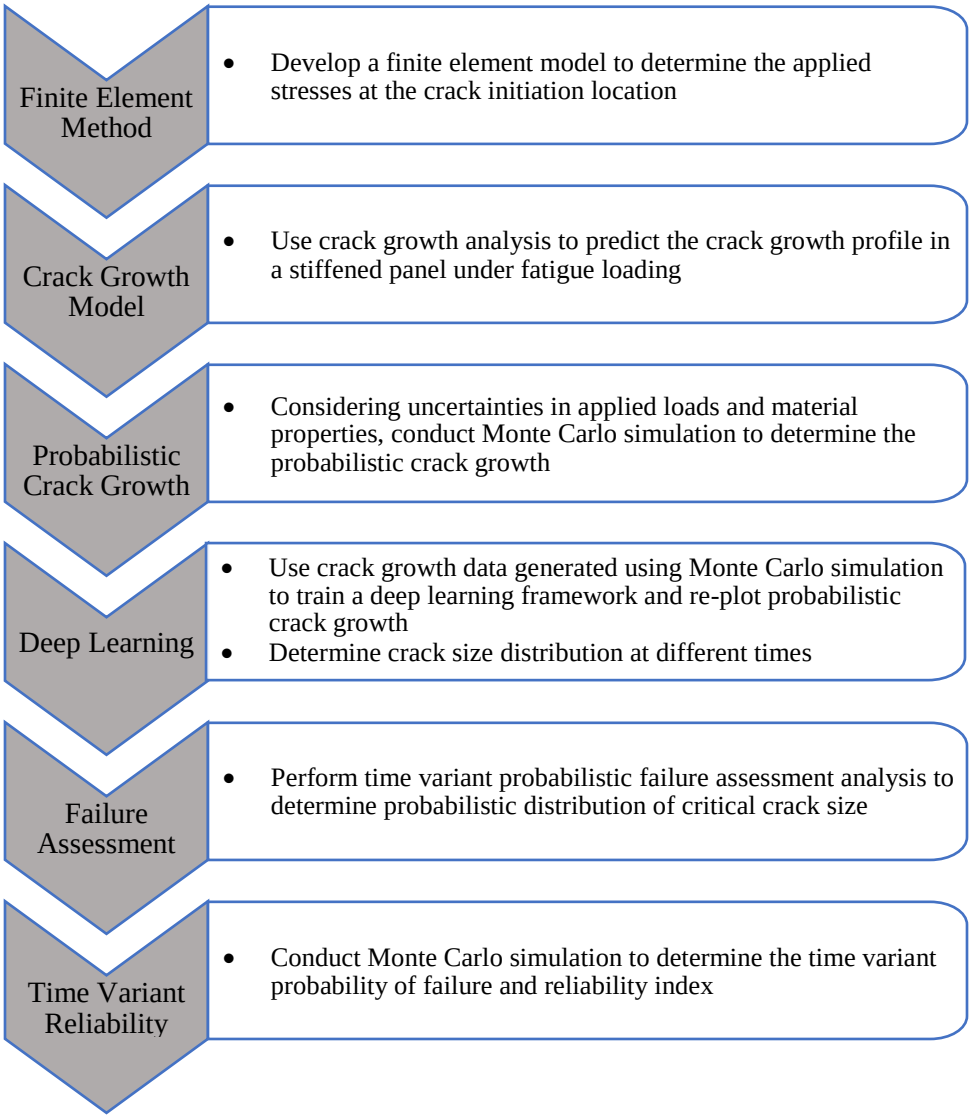

Figure 13 - Proposed probabilistic framework

CHAPTER III

ILLUSTRATIVE EXAMPLE

A three-lane bridge, adapted from the Federal Highway Administration Steel Bridge Design Handbook (FHA, 2012), is selected to illustrate the proposed fatigue reliability estimation framework. The superstructure of the selected bridge is a composite section with a 230 mm thick reinforced concrete deck on top of two trapezoid steel tub girders. It has a 13 meters wide roadway and a simply supported span of 40 meters. The cross-sectional dimensions are shown in Figure 14. The bottom flange of each of the girders has four longitudinal T stiffeners. Figure 15 shows the details of the longitudinal stiffeners of the box girder. The deck reinforced concrete has a strength of 28 MPa and the girder steel is ASTM A572 Gr. 50.

A finite element model of the bridge is constructed using SAP2000® v.19 (SAP2000, 2016) to determine the maximum and minimum stresses. The model was developed for one span of the bridge assuming pinned support conditions. It is constructed using a combination of shell and frame elements. The flanges and webs of the box girder are modelled as shell elements and the longitudinal stiffeners are modelled as frame elements. The finite element analysis provides the stresses experienced by the bridge under different configurations of live load. Figure 16 shows the finite element model developed. Figure 17 shows the AASHTO (AASHTO, 2017) fatigue truck loads, that are placed on the bridge to obtain the largest developed stress at mid-span. This

was conducted for one lane loaded, two lanes loaded, and three lanes loaded along with their respective multi-presence factors as tabulated in Table 4. The two-truck configuration resulted in the highest developed stress and is thus used. The stress under dead load of the structure is taken as σ_{min} while σ_{max} is the sum of the stresses due to dead load and the AASHTO fatigue truck load. For this analysis, $\sigma_{max} = 50.17$ MPa and $\sigma_{min} = 28.31$ MPa.

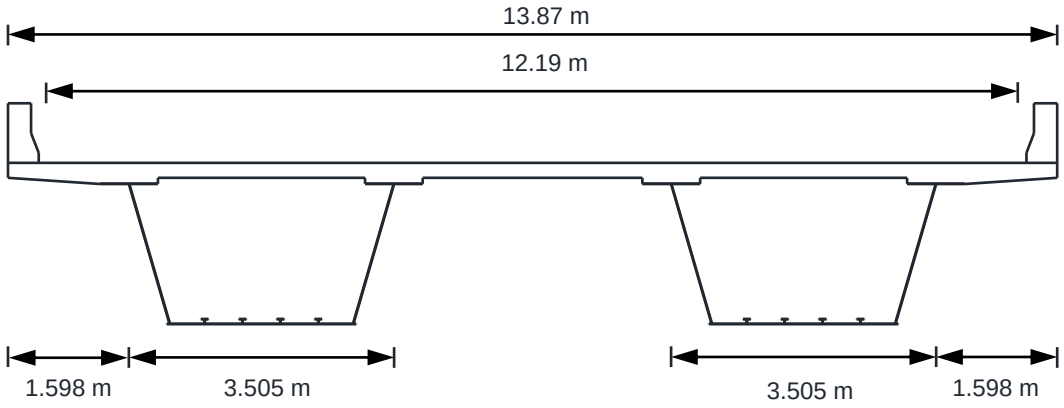

Fig. 14 - Bridge cross-section

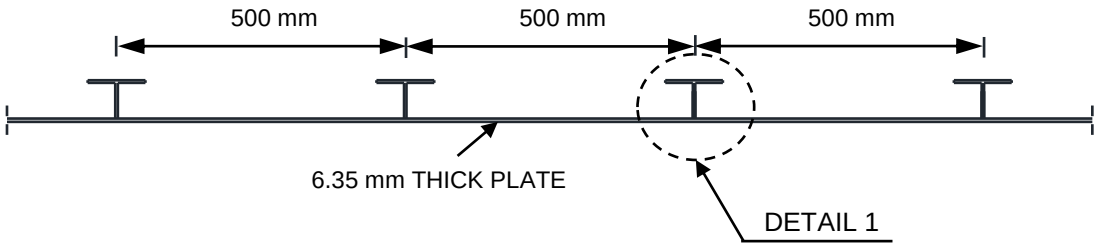

Fig. 15(a) - Stiffened bottom flange

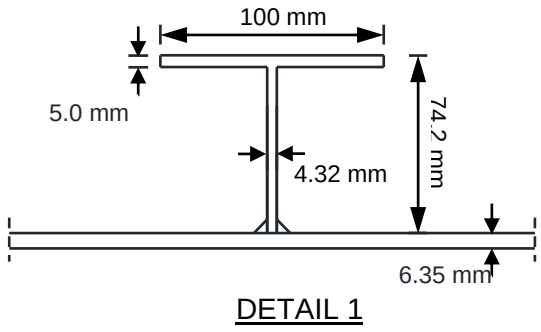

Fig. 15(b) - Stiffener detail

Table 4 - AASHTO multiple presence factors (AASHTO, 2017)

Multiple Presence Factors	
Number of Design Lanes	Multiple Presence Factor *m*
1	1.20
2	1.00
3	0.85
More than 3	0.65

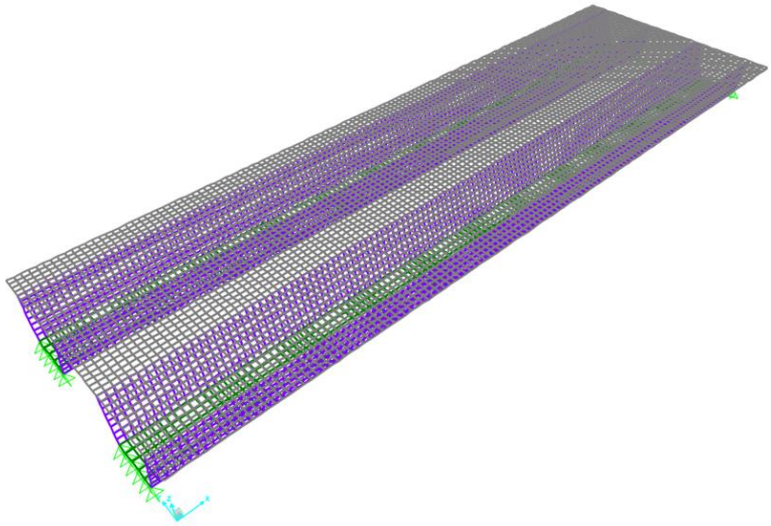

Fig. 16 - Finite element model

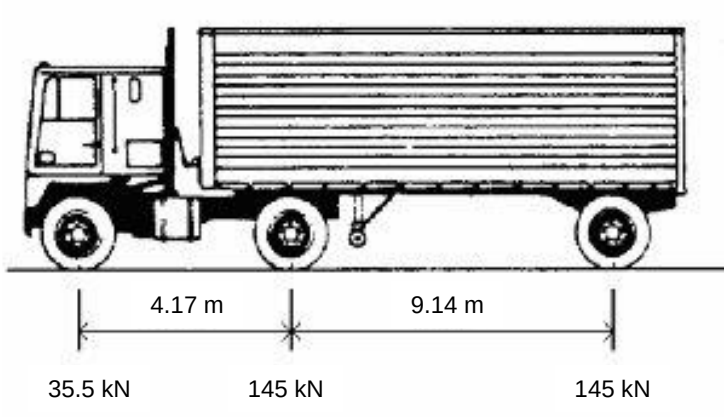

Fig. 17 - AASHTO fatigue truck

Stiffened Panel Coefficient

Equation (3) is used to model the crack growth through the bottom flange of the stiffened tub girder. The ΔK_{eff} is determined in accordance with the steps outlined in Figure 8. First, the stiffener restraint coefficient f_1 is determined using Equations (5-6) and severed stiffener effect, f_2 is determined using Equations (7-9). The stiffened panel coefficient is then assembled using Equation (10). Figure 18 shows f_1, f_2 and f_{st} for the case under consideration. As discussed, linear interpolation is executed from 0.95χ before the stiffener, to a point at a distance equal to the height of the stiffener ahead of it and is shown in Figure 19.

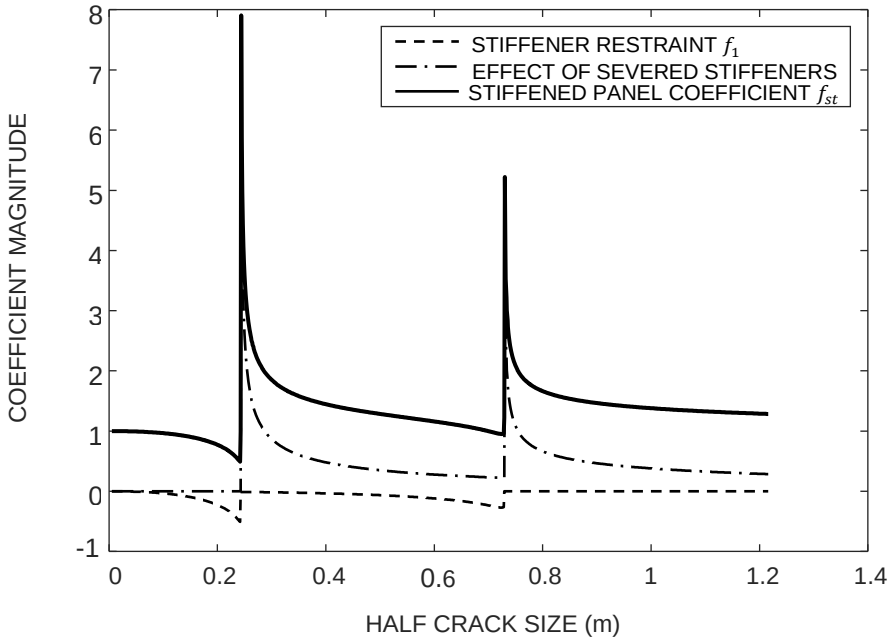

Fig. 18 - Formulation of stiffened panel coefficient

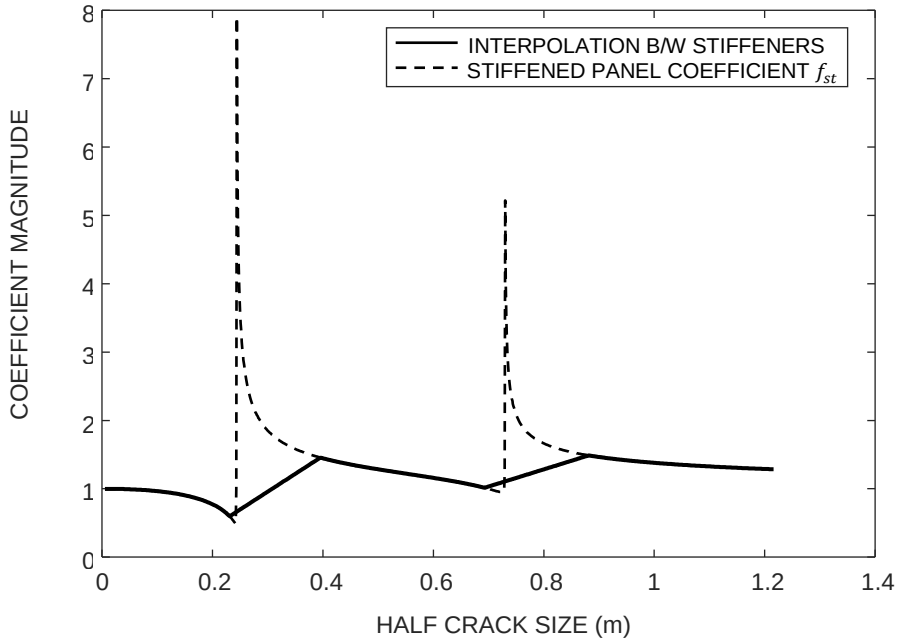

Fig. 19 - Linear interpolation between broken and intact stiffener

Residual Stress and Residual Stress Intensity Factor

The residual stress distribution along the panel can be modeled based on recommendations in Dexter and Pilarski (2000) and is plotted in Figure 20. It is seen that the residual stress distribution at the location of the stiffener is a triangle with base width of 3.5 times the thickness of the plate and the maximum stress is equal to the yield strength of the material i.e. 345 MPa. Using Equation (11), the residual stress intensity factor is evaluated and is plotted in Figure 21. Next, the effective stress intensity factor range is evaluated and the result is plotted in Figure 22. The value of the crack growth constant C is taken as 2.18×10^{-13} (Barsom and Rolfe, 1999) and material crack growth exponent m is taken as 3 (Barsom and Rolfe, 1999). Finally, the effective stress intensity factor range is used in Equation (3) to establish the deterministic crack growth profile through the stiffened panel over time which is plotted in Figure 23.

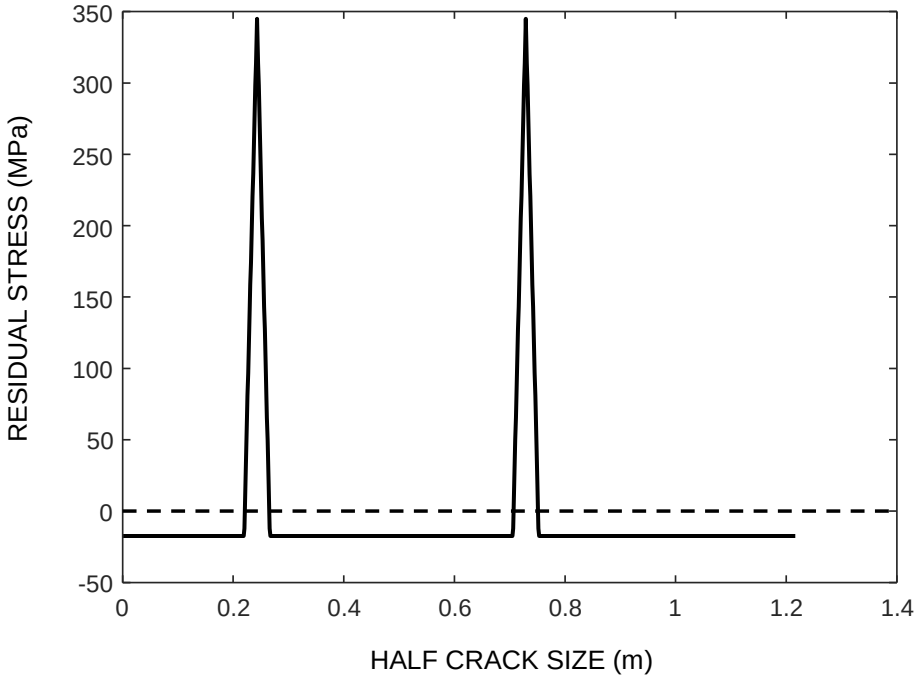

Fig. 20 - Residual stress distribution in the panel

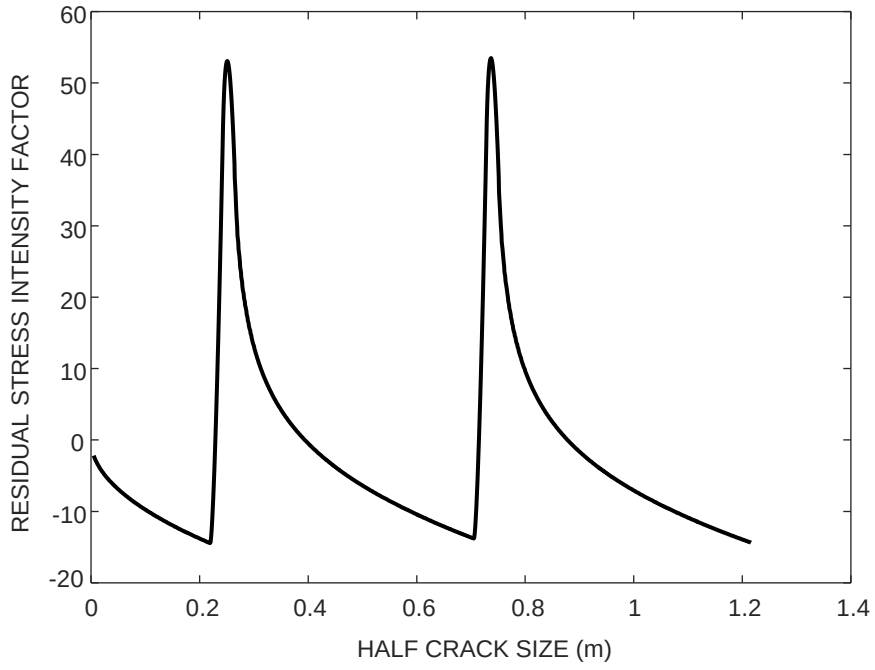

Fig. 21 - Residual stress intensity factor

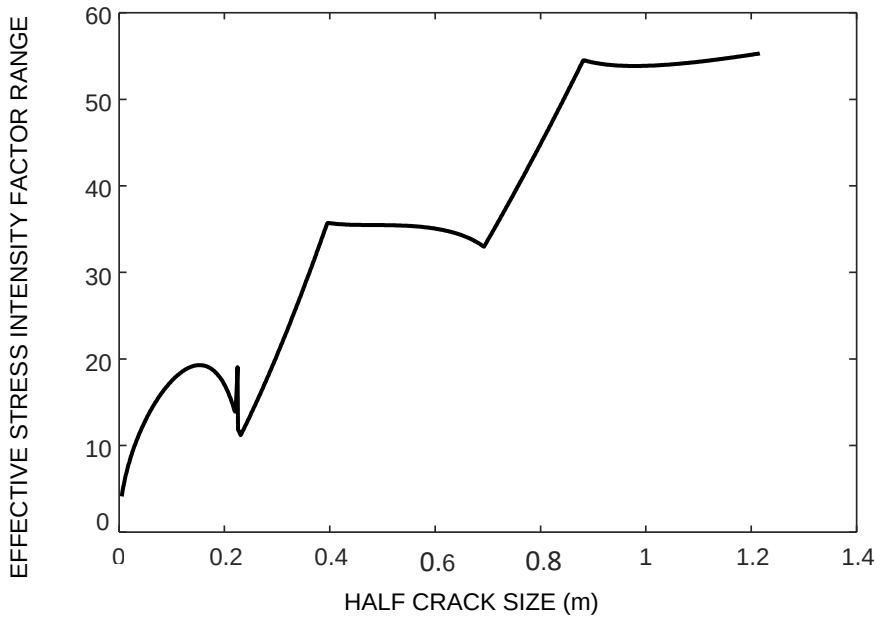

Fig. 22 - Effective stress intensity factor range

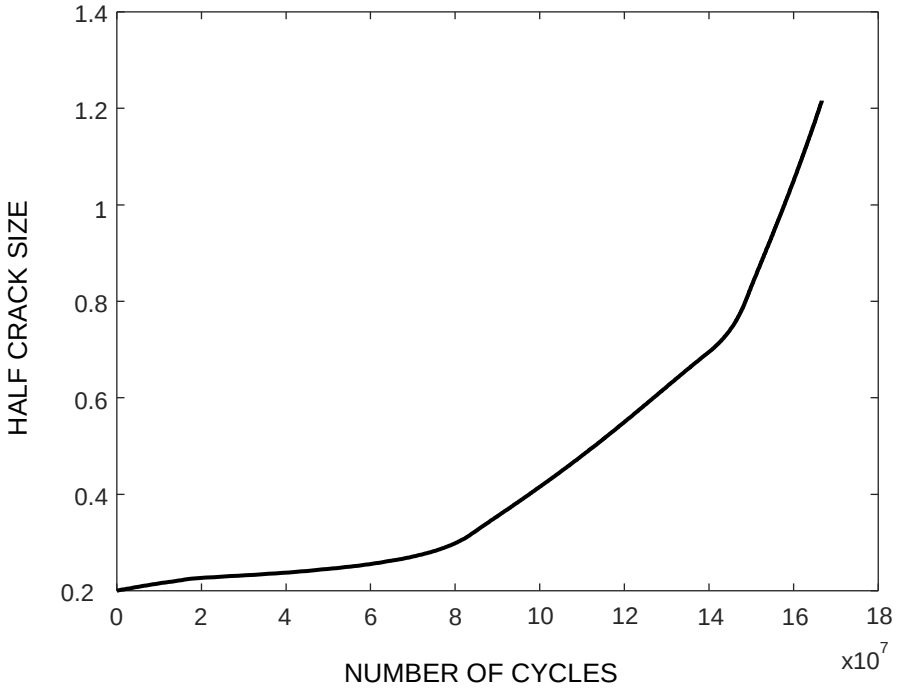

Fig. 23 - Crack growth profile

Probabilistic Crack Growth

To consider the effect of uncertainties in the applied loads, σ_{max} and σ_{min} are assumed to be normally distributed random variables with means of 50.17 MPa and 28.31 MPa respectively and coefficient of variance (COV) of 0.06 and 0.1 respectively. The material crack growth parameter C is assumed to follow a lognormal distribution with a mean of 2.18×10^{-13} and a coefficient of variance of 0.2 (Barsom and Rolfe, 1999). Random samples are generated for σ_{max}, σ_{min} and C using MATLAB 2018® random number generator, and Monte Carlo simulation is used to establish the crack growth for each sample and is shown in Figure 24. This simulation was performed on Dell OptiPlex 7050 workstation with Core i7-7700 CPU and 16 GB of RAM. It was observed that the computation time required to predict the crack growth associated with each sample was computationally expensive and time consuming. Only 1000 samples were generated in about 52 hours of computational run time. For Monte Carlo simulation, 1000 samples cannot accurately capture the sample space from all the regions in the probability distribution. Therefore, deep learning was used to reduce this time and generate larger number of samples.

Deep Learning

The crack size data generated from Monte Carlo simulation is used as an input data set for training the deep learning model. 20% of the data set is used as the training data and the remaining 80% is used for testing and verification. It is more efficient for neural networks to use scaled inputs as it takes fewer iterations to converge to a correct prediction (Heinz, 2017). Hence, the inputs are normalized with respect to the largest values in the data set, so that the training values remain between 0 and 1. For this study, the deep learning model is trained to find the time associated with different crack growth increments. The input parameters include stress intensity factor range ΔK_{eff}, crack growth constant C and the crack size a. The output parameter is the number of cycles N.

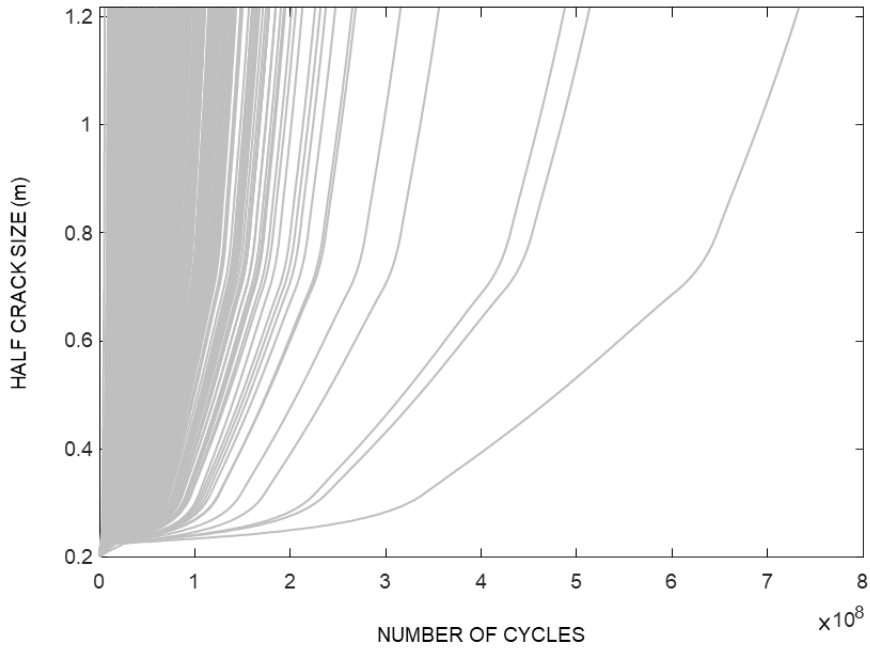

Fig. 24 - Probabilistic crack growth using Monte Carlo simulation

A session is created in TensorFlow to initiate and train a feed forward neural network. The network architecture consists of one input layer and 6 hidden layers and an output layer (Heinz, 2017). For error evaluation, the cost function uses the Mean Squared Error (MSE) method. To adjust the weights and bias values for the respective nodes, an Adam Optimizer is used (Kingma and Ba, 2014). The optimizer generates the gradients that determine the direction in which the weights and biases need to be adjusted to minimize the error. The results of the training model are compared to those of the analytical model at a sample with input parameters $\sigma_{max} = 54.68$ MPa, $\sigma_{min} = 24.23$ MPa and $C = 2.73 \times 10^{-13}$ as shown in Figure 25. A good agreement between the results from deep learning and those based on analytical results is observed.

Next, the trained model is used to generate a probabilistic crack growth profile using 100,000 predicted samples, as shown in Figure 26 and the crack size distribution can now be determined

for each time step. Since this is not directly available from the probabilistic analysis, distribution fitting is performed at each time instant using MATLAB® Distribution Fitting Toolbox, to determine these probabilistic distributions. It is observed that the crack size follows a Generalized Extreme Value Distribution. Figure 27 shows the distribution fitting of the samples of crack size at a selected time instant.

Probabilistic FAD Analysis and Time Variant Reliability Index

The probabilistic distribution of the critical crack size is required to determine the time variant reliability index. Probabilistic FAD analysis is performed to determine the distribution of the critical crack size. The reference stress, σ_{ref}, used for calculation of the load ratio, depends on the geometry and the stress concentrations around the flaw. Since the presented case is a complex geometry case, formulae from Annex P of BSI 7910 may not provide accurate results.

A crack is initiated in the FEM at the location of the highest stress in the lower flange of the tub girder by creating a fine mesh at that location and removing shell elements, simulating a crack. Static finite element analysis is then conducted to determine the stresses around the crack tip, which is taken to be the value of σ_{ref} (Tipple and Thorwald, 2012). This process is performed for incremental crack sizes up to a crack size of 2432 mm. Next, L_r is determined using Equation (13). Since A572 steel does not exhibit yield discontinuity, the assessment line will be determined using Equation (17). The fracture ratio K_r, is determined by employing applied stress intensity factor K_I, determined using the procedure described earlier (Dexter and Pilarski, 2003), which includes the effects of primary bending stresses and secondary stresses (i.e. applied forces and residual stresses). Assuming uncertainty in the yield strength and ultimate tensile strength of the material, multiple intersections between the assessment points and the assessment line will occur.

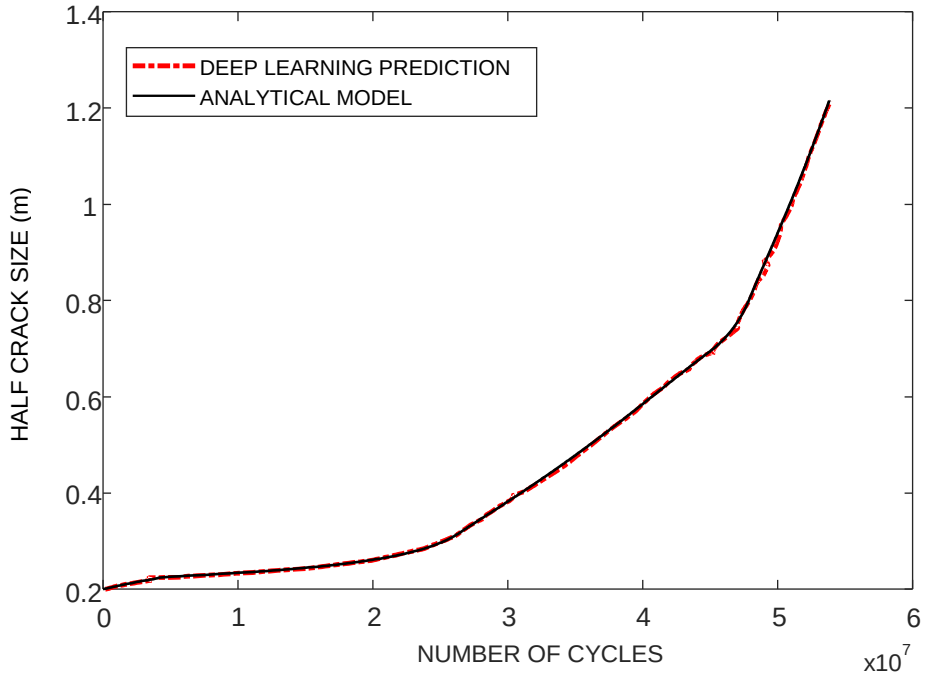

Fig. 25 - Verification of results using deep learning

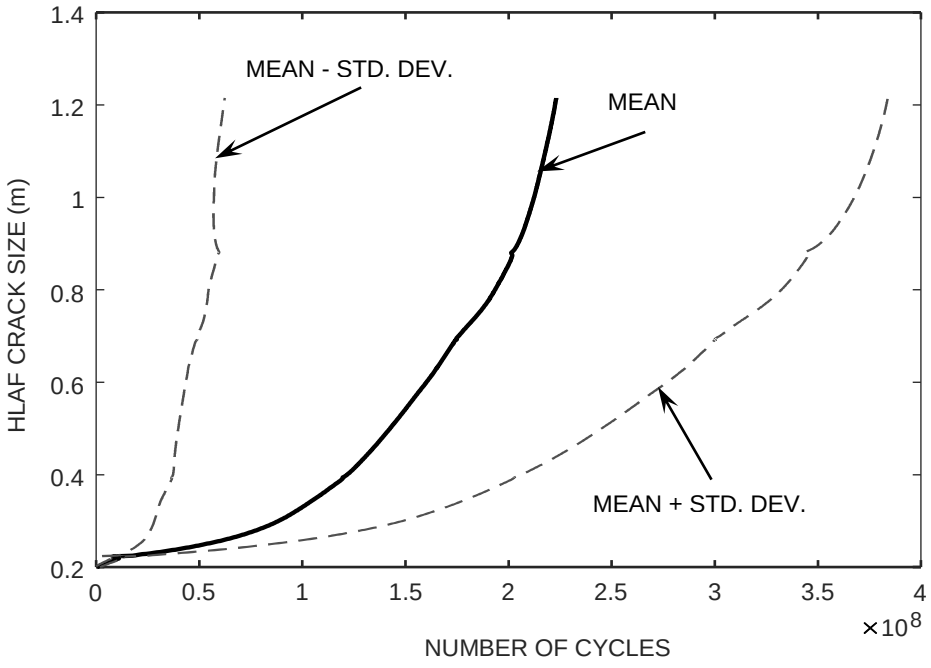

Fig. 26 - Probabilistic crack growth using deep learning

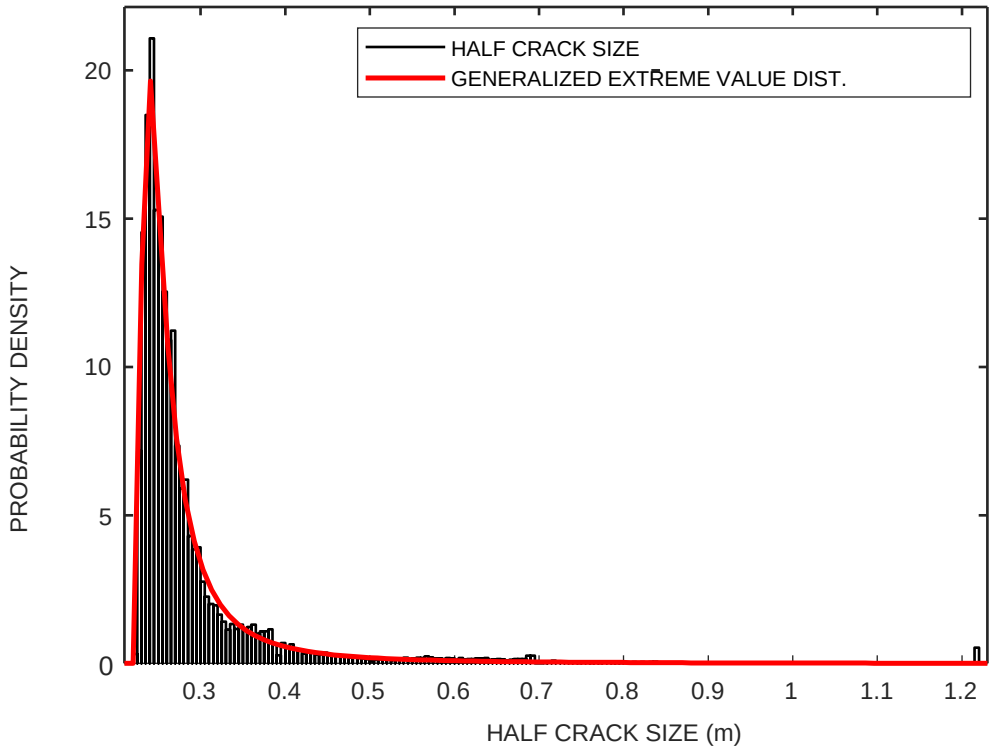

Fig. 27 - Distribution fit for instantaneous crack size at 35 million cycles

The yield strength is assumed to follow a lognormal distribution with a mean of 370 MPa and a COV of 0.07 and the tensile strength follows a lognormal distribution with a mean of 690 MPa and a COV of 0.04 (JCSS, 2001). A summary of the random parameters is shown in Table 5. A positive correlation of 0.75 is also assumed to exist between the tensile and yield strength (JCSS, 2001) Monte Carlo simulation is performed to plot the probabilistic Option 1 FAD as shown in Figure 28. It is observed that the assessment points lie in zone 3, indicating that the failure is dominated by plastic collapse. Next, a distribution fit can be performed to determine the distribution of the critical crack size using MATLAB® Distribution Fitting Toolbox. It was found that the critical crack size follows a normal distribution with a mean of 2.238 meters with a standard deviation of 0.036 meters. Figure 29 shows the distribution fit for the half critical crack size a_{cr}.

Table 5 - Summary of descriptors of random parameters

Parameter	Distribution	Mean	COV
Maximum stress, σ_{max} (MPa)	Normal	50.17	0.06
Minimum stress, σ_{min} (MPa)	Normal	28.31	0.1
Crack growth constant, C	Lognormal	2.18×10^{-13}	0.2
Yield strength, σ_Y (MPa)	Lognormal	370	0.07
Ultimate tensile strength, σ_u (MPa)	Lognormal	690	0.04

Next, Monte Carlo simulation is used to determine the probability of failure using Equation (21). Assuming the Average Daily Truck Traffic (ADTT) to be 2000 (Cheung and Li, 2003), the time dependent probability of failure is plotted against time and is shown in Figure 30. The plot shows that the probability of failure is very small during approximately the first 40 years of service. Subsequently the time variant reliability index can be determined using Equation (22) and is shown in Figure 31. Assuming 3.5 as the target reliability index (AASHTO, 2017), it is observed that the girder falls short of this value after approximately 48 years of service life. Setting other values as threshold reliability values will result in different values of service life. Table 6 shows the reliability based service life associated with different reliability thresholds.

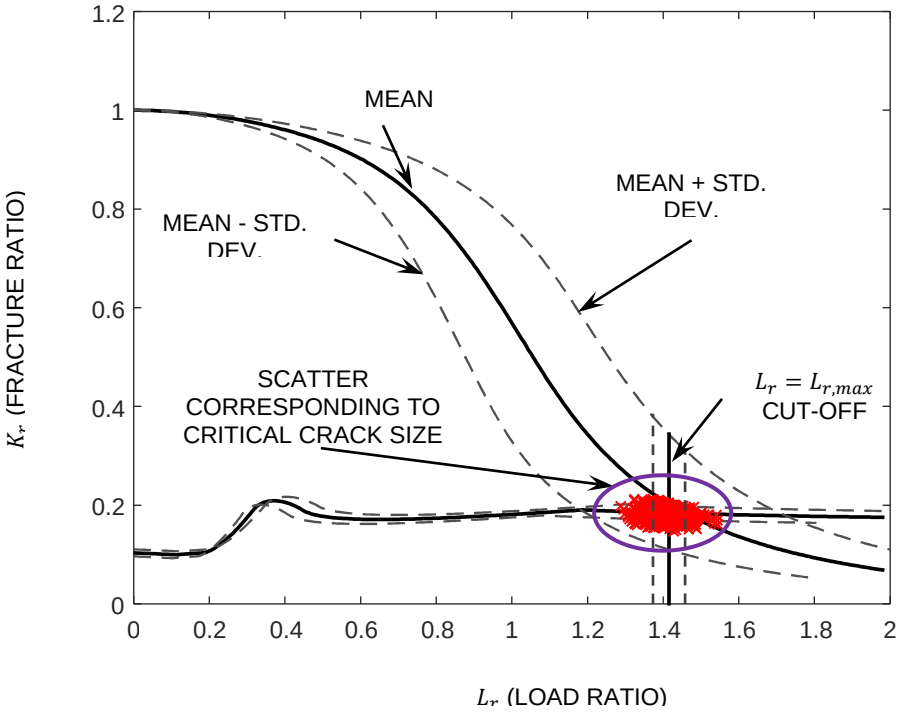

Fig. 28 - Probabilistic Option 1 FAD analysis showing scatter of critical points

Table 6 - Service life associated with different reliability threshold values

Reliability Threshold	**Service Life (Years)**
4.0	42
3.5	45
3.0	54
2.5	68
2.0	83

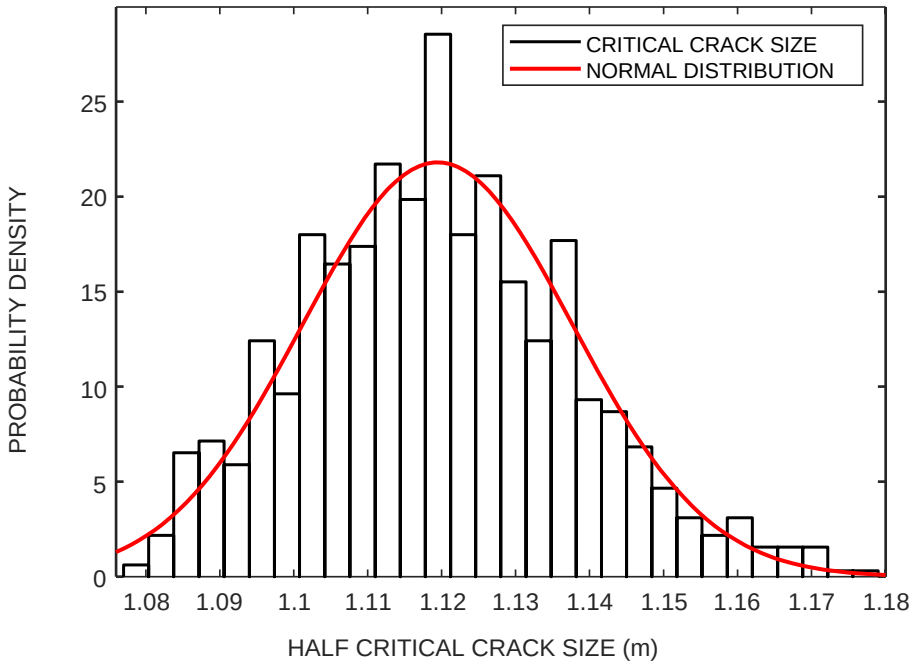

Fig. 29 - Distribution fit for critical crack size

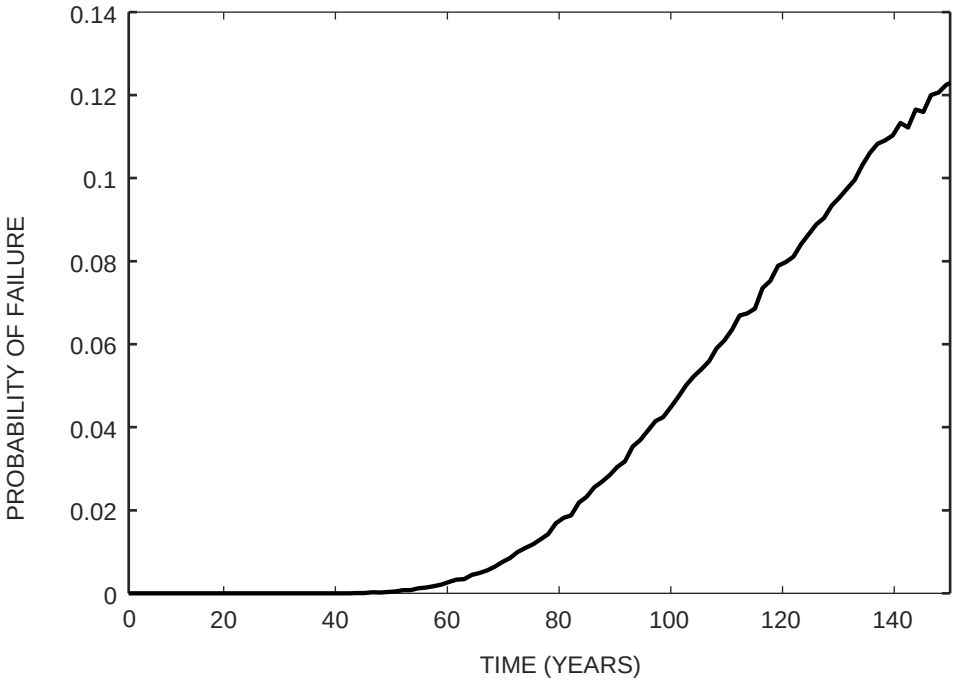

Fig. 30 - Time variant probability of failure

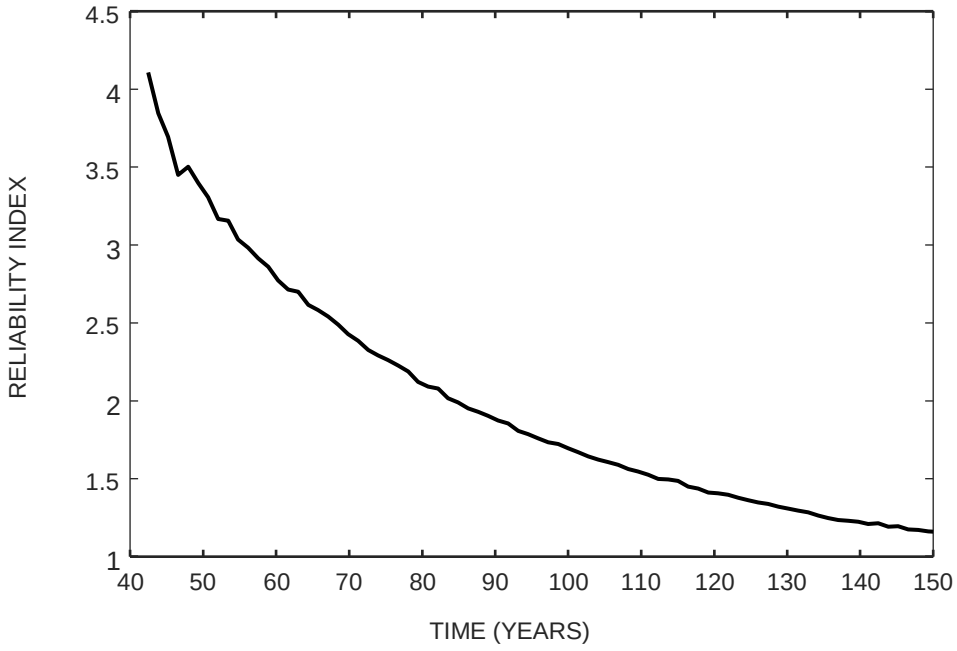

Fig. 31 - Time variant reliability index

CHAPTER IV

CONCLUSIONS AND FUTURE WORK

Conclusions

This study presented a probabilistic framework to quantify the time variant reliability index of stiffened panels under growing fatigue cracks. This approach employs LEFM to determine probabilistic crack growth profile through the stiffened plates considering uncertainties in loads and material properties. To establish the time variant reliability profile, the critical crack size is required. In this work the critical crack size was determined using a probabilistic failure assessment diagram analysis, whose descriptors were quantified using Monte Carlo simulation. It was observed that this entire simulation process was computationally expensive to accurately capture the performance of the structure. A deep learning framework, TensorFlow, was trained and verified using the sparse data available from the analytical model. The results of the deep learning framework showed very good agreement with the analytical ones. The trained model enabled a large number of samples to be used to establish the probabilistic crack growth profile, using Monte Carlo simulation. A performance function was defined in terms of the time variant crack size and the critical crack size to quantify the probability of failure and reliability index. A stiffened bridge tub girder was used to illustrate the approach. The following conclusions can be drawn:

- Failure assessment diagrams are a useful to determine critical crack size in probabilistic

fatigue analysis. For these types of cracks, the main failure mode was identified as ductile failure. These cracks can grow into a substantial length before failure. This can be attributed to the high material toughness and the inherent redundancy of the stiffened structures.

- The Generalized Extreme Value (GEV) distribution was found to provide the best fit of crack size data at different tie instances.
- It was observed that the structural reliability during the first 40 years was very high. Computing the reliability index during these years requires a larger number of simulations.
- Deep learning can be effectively used to accelerate the stochastic analyses to determine probabilistic distribution of the instantaneous crack size over time. This process can be applied to other structural problems such as corrosion models.
- For the analyzed case study, traditional Monte Carlo simulation would require approximately 5500 hours of computational run time whereas with deep learning this time is reduced to 43 hours.
- The proposed approach that integrates deep learning algorithms in probabilistic analyses can be applied to other structural engineering applications such as fragility analysis, structural performance under environmental corrosion and seismic response of structures.

Future Work

The following suggestions are recommended for future studies to better utilize the proposed framework for evaluating structural performance under uncertainty:

- The FAD analysis for this study was performed using Option 1 analysis. More advanced options can be employed by collecting material properties such as true stress-strain data
- The adopted analytical model considers the crack growth under constant amplitude loading. However, the stress cycles experienced by structures are highly variable. Modifications should be made to this model by incorporating the effects of overload and underload to predict crack growth under variable amplitude loading.

REFERENCES

AASHTO, LRFD. 2017. Bridge design specifications. American Association of State Highway and Transportation Officials, Washington, DC.

ABADI, M., BARHAM, P., CHEN, J., CHEN, Z., DAVIS, A., DEAN, J., DEVIN, M., GHEMAWAT, S., IRVING, G. & ISARD, M. Tensorflow: a system for large-scale machine learning. OSDI, 2016. 265-283.

ADMINISTRATION, F. H. 2012. Design Example 4: Three Span Continuous Straight Composite Steel Tub Girder Bridge. *Steel Bridge Design Handbook,* 24.

ALBRECHT P., YAMADA, K., Rapid calculation of stress intensity factors, *J Struct Div, Proc ASCE,* 103 (ST2) (1977), pp. 377-389

AL-RFOU, R., ALAIN, G., ALMAHAIRI, A., ANGERMUELLER, C., BAHDANAU, D., BALLAS, N., BASTIEN, F., BAYER, J., BELIKOV, A. & BELOPOLSKY, A. 2016. Theano: A Python framework for fast computation of mathematical expressions.

ASCE COMMITTEE ON FATIGUE AND FRACTURE RELIABILITY OF THE COMMITTEE ON STRUCTURAL SAFETY AND RELIABILITY OF THE STRUCTURAL DIVISION, 1982. *Committee on Structural Safety and Reliability of the Structural Division, J. ST. Div. ASCE ST,* 1.

BARSOM, J. M. & ROLFE, S. T. 1999. *Fracture and fatigue control in structures: applications of fracture mechanics*.

BSI 2013. Guide to methods for assessing the acceptability of flaws in metallic structures. *BS 7910: 2013*.

CHEUNG, M. S. & LI, W. 2003. Probabilistic fatigue and fracture analyses of steel bridges. *Structural Safety,* 25**,** 245-262.

DEXTER, R.J., Pilarksi, P.J., Effect of welded stiffeners on fatigue crack growth rate, SSC-413, Washington DC. *Ship Structure Committee, 2000.*

DEXTER, R.J. & PILARSKI, P. 2002. Crack propagation in welded stiffened panels. *Journal of Constructional Steel Research,* 58**,** 1081-1102.

DEXTER, R. J., PILARSKI, P. J. & MAHMOUD, H. N. 2003. Analysis of crack propagation in welded stiffened panels. *International Journal of Fatigue,* 25**,** 1169-1174.

FAULKNER D. A review of effective plating for use in the analysis of stiffened plating in bending and compression. *J Ship Res* 1975;19:1–17.

FISHER, J. W. 1984. *Fatigue and fracture in steel bridges. Case studies*.

HAN, M. K. & RAMULU, M. Fatigue Life Prediction of Ship Welded Materials. Key Engineering Materials, 2005. Trans Tech Publ, 743-749.

HEINZ, S., 2017. A simple deep learning model for stock price prediction using TensorFlow. *ML Review, https://medium.com/mlreview/a-simple-deep-learning-model-for-stock-price-prediction-using-tensorflow-30505541d877*

ISIDA, M. 1973. Analysis of stress intensity factors for the tension of a centrally cracked strip with stiffened edges. *Engineering Fracture Mechanics,* 5**,** 647-665.
JCSS, 2001. Part 3: Resistance Models. Joint Committee of Structural Safety.
JIA, Y., SHELHAMER, E., DONAHUE, J., KARAYEV, S., LONG, J., GIRSHICK, R., GUADARRAMA, S. & DARRELL, T. Caffe: Convolutional architecture for fast feature embedding. Proceedings of the 22nd ACM international conference on Multimedia, 2014. ACM, 675-678.
KETKAR, N. 2017. Introduction to Keras. Deep Learning with Python: A Hands-on Introduction. Berkeley, CA: Apress.
KIM, S., FRANGOPOL, D. M. & SOLIMAN, M. 2013. Generalized probabilistic framework for optimum inspection and maintenance planning. *Journal of Structural Engineering,* 139**,** 435-447.
KINGMA, D. P. & BA, J. 2014. Adam: A method for stochastic optimization. *arXiv preprint arXiv:1412.6980*.
KONDO, J. & OSTAPENKO, A. 1964. Tests on longitudinally stiffened plate panels with fixed ends, July 1964.
KWON, K., FRANGOPOL, D. M. & SOLIMAN, M. 2012. Probabilistic Fatigue Life Estimation of Steel Bridges by Using a Bilinear S-N Approach. *Journal of Bridge Engineering,* 17**,** 58-70.
LECUN, Y., BENGIO, Y. & HINTON, G. 2015. Deep learning. nature, 521, 436.
LIU, M., FRANGOPOL, D. M. & KWON, K. 2010. Fatigue reliability assessment of retrofitted steel bridges integrating monitored data. *Structural Safety,* 32**,** 77-89.
LU, Z. & LIU, Y. 2010. Small time scale fatigue crack growth analysis. *International Journal of Fatigue,* 32**,** 1306-1321.
MAHMOUD, H. & RIVEROS, G. 2014. Fatigue reliability of a single stiffened ship hull panel. *Engineering Structures,* 66**,** 89-99.
MAHMOUD, H. N. & DEXTER, R. J. 2005. Propagation rate of large cracks in stiffened panels under tension loading. *Marine Structures,* 18**,** 265-288.
MCMILLAN, J. & PELLOUX, R. 1967. Fatigue crack propagation under program and random loads. *Fatigue Crack Propagation.* ASTM International.
MOHANTY, J., MAHANTA, T., MOHANTY, A. & THATOI, D. 2015. Prediction of constant amplitude fatigue crack growth life of 2024 T3 Al alloy with R-ratio effect by GP. *Applied Soft Computing,* 26**,** 428-434.
NOWAK, A. S. 1993. Live load model for highway bridges.
NUSSBAUMER, A. 1994. Propagation of long fatigue cracks in multi-cellular box beams.
NUSSBAUMER, A. C., FISHER, J. W. & DEXTER, R. J. 1999. Behavior of long fatigue cracks in cellular box beam. *Journal of Structural Engineering,* 125**,** 1232-1238.
OSGOOD, W. R. 1954. *Residual stresses in metals and metal construction,* Reinhold Publishing Corporation.
PARIS, P. & ERDOGAN, F. 1963. A critical analysis of crack propagation laws. *Journal of basic engineering,* 85**,** 528-533.
POE, C. 1971. Fatigue crack propagation in stiffened panels. *Damage Tolerance in Aircraft Structures.* ASTM International.
RICE, J. 1968. Mathematical Analysis in the Mechanics of Fracture in Fracture: An advanced treatise, Vol. II, Mathematical Fundamentals, ed. Liebowitz H., 191-311. Academic Press, New York.
ROOKE, D. P. & CARTWRIGHT, D. J. 1976. Compendium of stress intensity factors. Procurement Executive, Ministry of Defence. H. M. S. O. 1976, 330 p(Book).
RYBICKI, E. F. & KANNINEN, M. F. 1977. A finite element calculation of stress intensity factors by a modified crack closure integral. Engineering fracture mechanics, 9, 931-938.
SAP2000 Analysis Reference Computers and Structures, Inc, Berkeley (CA) (2016)

SOCHER, R., LIN, C. C., MANNING, C. & NG, A. Y. Parsing natural scenes and natural language with recursive neural networks. Proceedings of the 28th international conference on machine learning (ICML-11), 2011. 129-136.
SOLIMAN, M., FRANGOPOL, D. M. & KIM, S. 2013. Probabilistic optimum inspection planning of steel bridges with multiple fatigue sensitive details. *Engineering Structures,* 49**,** 996-1006.
STERN, R. E., SONG, J. & WORK, D. B. 2017. Accelerated Monte Carlo system reliability analysis through machine-learning-based surrogate models of network connectivity. *Reliability Engineering & System Safety,* 164**,** 1-9.
TIPPLE, C. & THORWALD, G. Using the failure assessment diagram method with fatigue crack growth to determine leak-before-rupture. 2012 SIMULIA Community Conference, Providence, Rhode Island, 2012.
VENKATESAN, K. R. 2016. Subcycle fatigue crack growth formulation for constant and variable amplitude loading, Arizona State University.
WANG, W., LIU, C. & ZHOU, S. 1999. On the probabilistic failure assessment diagram. *International journal of pressure vessels and piping,* 76**,** 653-662.
WOLF, E. 1971. The significance of crack closure, damage tolerance in aircraft structures. *Journal of American Society for Testing of Materials, ASTM STP,* 486.
XIAO, Z.-G., YAMADA, K., INOUE, J. & YAMAGUCHI, K. 2006. Fatigue cracks in longitudinal ribs of steel orthotropic deck. *International Journal of Fatigue,* 28**,** 409-416.
ZHANG, W., BAO, Z., JIANG, S. & HE, J. 2016. An artificial neural network-based algorithm for evaluation of fatigue crack propagation considering nonlinear damage accumulation. *Materials,* 9**,** 483.
ZHAO, J.-P., HUANG, W.-L. & DAI, S.-H. 1997. A new concept: probabilistic failure assessment diagram. *International journal of pressure vessels and piping,* 71**,** 165-168.
ZHAO, Z., HALDAR, A. & BREEN, F. L. 1994a. Fatigue Reliability Evaluation of Steel Bridges. *Journal of Structural Engineering,* 120**,** 1608-1623.
ZHAO, Z., HALDAR, A. & BREEN JR, F. L. 1994b. Fatigue-reliability evaluation of steel bridges. *Journal of structural engineering,* 120**,** 1608-1623.
ZIO, E. & DI MAIO, F. 2012. Fatigue crack growth estimation by relevance vector machine. *Expert Systems with Applications,* 39**,** 10681-10692.

VITA

Haider Ali

Candidate for the Degree of

Master of Science

Thesis: ACCELERATED FATIGUE RELIABILITY ANALYSIS OF STIFFENED SECTIONS USING DEEP LEARNING

Major Field: Civil Engineering

Biographical:

Education:

Completed the requirements for the Master of Science in Civil Engineering at Oklahoma State University, Stillwater, Oklahoma in December, 2018.

Completed the requirements for the Bachelor of Science in Civil Engineering at National University of Sciences and Technology, Islamabad, Pakistan in 2014.